Azimuthal Anisotropy Before Major Earthquakes In Japan From Shear Wave Splitting Analysis

By

Long Minh Ho

A Thesis Submitted to the Department of Earth and Atmospheric Sciences,

College of Natural Sciences and Mathematics

In Partial Fulfillment of the Requirements for the Degree of

Master of Science

In Geophysics

Chair of Committee: Aibing Li

Committee Member: Yingcai Zheng

Committee Member: Fenglin Niu

University of Houston

August 2021

ACKNOWLEDGEMENTS

Many things have happened this recent year, and I would have never made it without the help of many people.

First and foremost, my sincere gratitude to my advisor, Dr. Aibing Li. Thank you for showing me the world of seismology. Your feedback and support helped me through the ups and downs of doing research. Also, I would like to thank my committee members, Dr. Yingcai Zheng and Dr. Fenglin Niu, for their thoughtful comments on my thesis. I would like to thank the cohort of my research group. Thank you all for being great and supportive friends.

Lastly, my heartfelt gratitude goes to my family-Dad, Mom, and my grandparents. Thank you for your unconditional support and belief in me. Thank you, Mom, for all your encouragement stories, which help brighten my day.

ABSTRACT

Precursory anisotropy change before a major earthquake remains a controversial topic in earthquake seismology. Japan is an ideal place to study this topic because it experiences numerous large earthquakes and has a dense seismic network. We analyze shear-wave splitting (SWS) data from foreshocks recorded at four Hi-net seismic stations (JUOH, ASGH, SKGH, and TYNH) for four major earthquakes in Fukushima, Shizuoka, Tottori, and Kumamoto. SWS parameters (fast polarization direction and delay time) are calculated using a semi-automatic algorithm. The average fast directions at the four stations are either parallel to the local maximum horizontal stress orientation or the fault strike, consistent with previous studies. Both SWS parameters do not show noticeable temporal variations before large earthquakes at station JUOH, ASGH, and TYNH. At station SKGH in Tottori, the delay time varies randomly within a small range for most of the foreshocks that occurred from 25 days to 1 day before the main earthquake. A sharp jump of delay time (0.03 s) is observed within two hours between two groups of events before the mainshock in Tottori. The earlier group of events are relatively far from the mainshock, while the latest foreshocks are very close to the mainshock, indicating the region near the major earthquake is more anisotropic and evidencing a precursory anisotropy change. Our observations suggest that it is possible to observe anisotropy changes before large earthquakes when there are favorable foreshock datasets, although the success rate is low. More SWS measurements from foreshocks need to be conducted to corroborate the findings in this study.

TABLE OF CONTENTS

LIST OF TABLES

LIST OF FIGURES

CHAPTER 1

INTRODUCTION

Earthquakes have been around for billions of years, with the earliest descriptive records to trace back to over 3000 years ago. Throughout history, the Earth has revealed its unpredictable and dynamic nature. Despite numerous studies of earthquakes during the 19^{th} and 20^{th} centuries, our understanding of earthquakes and earthquake prediction still fall behind other scientific fields. The difference is clear when we look at the stark contrast between earthquake prediction and weather forecast. However, thanks to recent advances in technology, seismologists have made remarkable progress in observing, data processing, modeling, and analyzing seismic data, broadening our scientific understanding of earthquake processes. Due to the Earth's heterogeneous structure and the complexity of the seismic sources, the journey to better understand earthquakes' behavior is still a long way to go. Numerous methods have been applied to study earthquake's precursory changes. Among those methods is the use of shear wave splitting to measure anisotropy prior to major earthquakes.

Seismic anisotropy is defined as the velocity of a seismic wave depends on its polarization or propagation direction. Research concerning seismic anisotropy varies from laboratory measurements of the elastic properties of rocks and minerals to seismological observations of the Earth's interior structure (Kaneshima, 1995). Upper mantle anisotropy is believed to be the result of lattice preferred orientation (LPO) of olivine. Meanwhile, in the upper crust, brittle tensile cracks are the main cause of anisotropy, as they are predominantly aligned parallel to the maximum compressive stress (Fig. 1). However, brittle tensile cracks are unlikely to appear in the lower crust, and the mantle as increasing pressure closes all microcracks (Kaneshima, 1995).

Shear wave splitting (SWS) can help detect spatial and temporal variations in the stress field (Crampin, 1987; Peacock et al., 1988). A shear wave splits into two orthogonal components with different velocities as it travels through an anisotropic medium (Fig. 1). There are two splitting parameters defined as the fast direction and the delay time. The fast direction is the polarization orientation of the fast traveling component, while the delay time is the time between the fast and the slow components. Kaneshima (1990) investigated SWS in Japan and agreed that the fast directions were generally consistent with the regional stress field. Since SWS can be affected by the stress field, studying the temporal variations can help monitor the stress build-up and release of major earthquakes (Crampin et al., 1990; Li et al., 1999). Recent studies suggest massive earthquakes may contain foreshocks that act as imminent precursors before the mainshock, as observed in the 2011 Tohoku earthquake (Kamiyama et al., 2016; Pritchard et al., 2020). Shear wave splitting parameters measured from these foreshocks may provide clues for the mainshocks.

The focus of this thesis is investigating precursory changes of SWS parameters before larger earthquakes with $M_w>6.0$ in Japan. Due to generally insufficient foreshocks before large earthquakes, there are only a few places in the world where this type of study can be conducted (Crampin et al., 1999; Peacock et al., 1988; Savage et al., 2016). We chose Japan as our study area because of its dense seismic networks and pronounced seismicity. In the past, only a limited number of studies on temporal changes using shear wave splitting have been conducted in Japan (Saiga et al., 2003; Hiramatsu et al., 2005). The advancement of computational resources and a large amount of seismic data recorded in recent years enabled us to conduct a more comprehensive analysis of shear wave splitting in Japan.

In the following chapters, we present our study and analysis conducted in different regions in Japan. Chapter 2 summarizes Japan's geological history and tectonic settings and reviews previous research using the shear wave splitting method. Chapter 3 explains the data's origin, including the distribution of seismic stations, our selected study areas, and the selection of events used for SWS analysis. Chapter 4 illustrates how we process the SWS data, estimate the errors, and controls the quality of results. In Chapter 5, we present and explain our results obtained from the SWS analysis. Lastly, in Chapter 6, we integrate Chapter 5 with previous studies, discuss interesting observations, and draw conclusions.

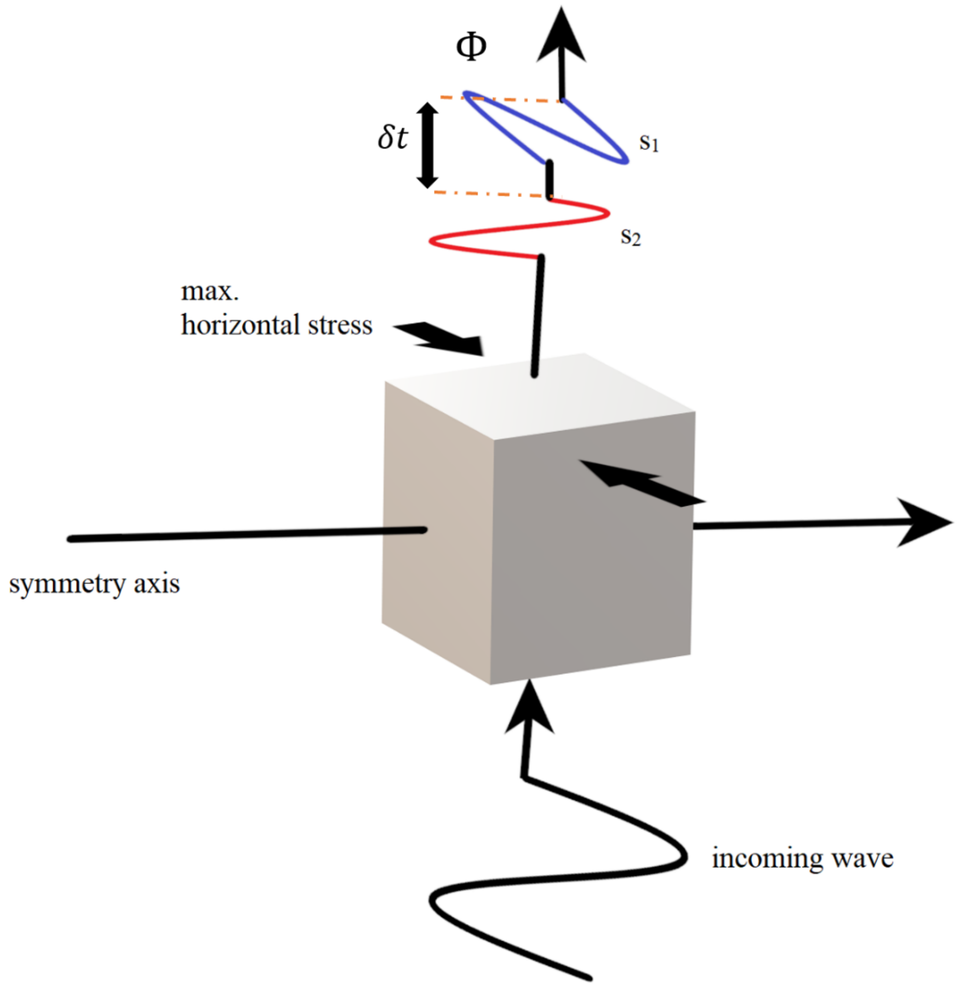

Figure 1. Schematic illustration of shear wave splitting through an anisotropic medium. The incoming shear wave splits into two orthogonal components, a fast shear wave (s_1) and a slow wave (s_2). The resulted splitting parameters are ϕ, the polarization direction of the fast shear wave, and δt, the time delay between the fast and slow wave. Diagram modified from Gao and Crampin (2004).

CHAPTER 2

TECTONIC SETTINGS AND PREVIOUS STUDIES

2.1 Tectonic History of Japan

Japan's tectonic history was initiated by the breakup of the Rodinia supercontinent around 750 Ma. Around 500 Ma, the Paleo-Pacific oceanic plate started to subduct under the continental plate. Henceforth, Japan has been situated on the convergent margin of East Asia (Wakita, 2013). Due to this tectonic setting, Japan has been experienced various tectonic events, including arc volcanism, subduction-accretion, back-arc spreading, and arc-arc collision (Wakita, 2013; Isozaki et al., 2011). The current tectonic of the Japan arc system is characterized by E-W compression that started during the late Pliocene to early Quaternary (Taira, 2001). There are five interacting plates around Japan: the Eurasia, Okhotsk, Amur, Pacific, and Philippines Sea plates (Taira, 2001) (Fig. 2). The subduction of the Pacific plate at the Kuril arc results in the Kuril forearc sliver. The Kuril forearc sliver migrated westward to form the Hidaka collision zone in central Hokkaido (Taira, 2001). The Pacific plate subducts underneath northeastern Honshu to the east, while the Amur plate subducts underneath the Okhotsk plate to the west (Taira, 2001). The Philippine Sea plate's oblique subduction results in the westward migration of the Nankai forearc sliver (Taira, 2001). The right boundary of the Nankai forearc sliver is the Median Tectonic Line (MTL), a right-lateral strike-slip fault. The sliver extends westward to the forearc of the Ryukyu arc, which is paired with a rifting back-arc basin, the Okinawa trough (Taira, 2001).

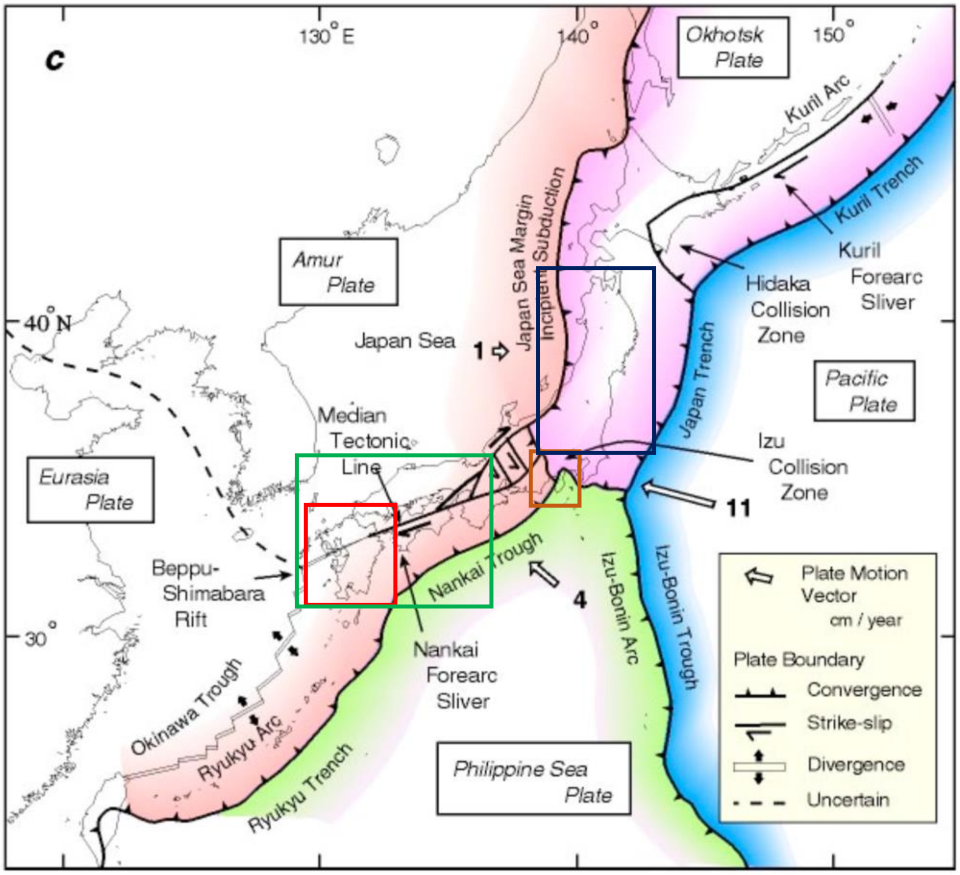

Figure 2. Tectonic map of Japan. Thick lines with triangle teeth represent convergence zones. Thick lines with horizontal arrows show strike-slip faults. Blank rectangles with diverging arrows show divergence zones. Different colors indicate different tectonic plates. Pink-Amur Plate; Purple-Okhotsk Plate; Blue-Pacific Plate; Green-Philippine Sea Plate. (Map from Taira (2001)). Different color boxes mark the regional tectonics show in figures 3-6. Red-Kyushu; Green-Southwest Japan; Brown-Shizuoka; Navy Blue-Northeast Japan.

2.1.1 Southwest Japan

Southwest Japan is a geologically and tectonically complex region of accreted terranes (Barber, 1982). After a delay in subduction from 10-6 Ma, the Philippine Sea plate resumed subduction at 6 Ma. The difference in the arc orientation resulted in the normal subduction beneath the Ryukyu Arc through the Ryukyu Trench and oblique subduction of the Philippine Sea plate beneath the Nankai Trough (Kamata and Kodama, 1994; Kamata, 1999). The MTL separated two major structural zones in Southwest Japan, an Outer (Pacific) and an Inner (Sea of Japan) Zone (Fig. 3). It extends 900 km in an E-W direction and contains numerous fault systems forming a 10-km wide shear zone. The oblique subduction of the Philippine Sea plate accelerated the dextral slip on the MTL, which caused a northward shift of the western end of the MTL (Kamata, 1999; Nakamura et al., 1987). Shallow earthquakes' focal mechanisms and SWS measurements show that the axis of maximum principal stress in Southwest Japan is in an E-W direction (Iio 1996; Kaneshima 1990). Towards the western margin of the Southwest Japan Arc (northern Kyushu and northern Chugoku), the number of strike-slip faults increases.

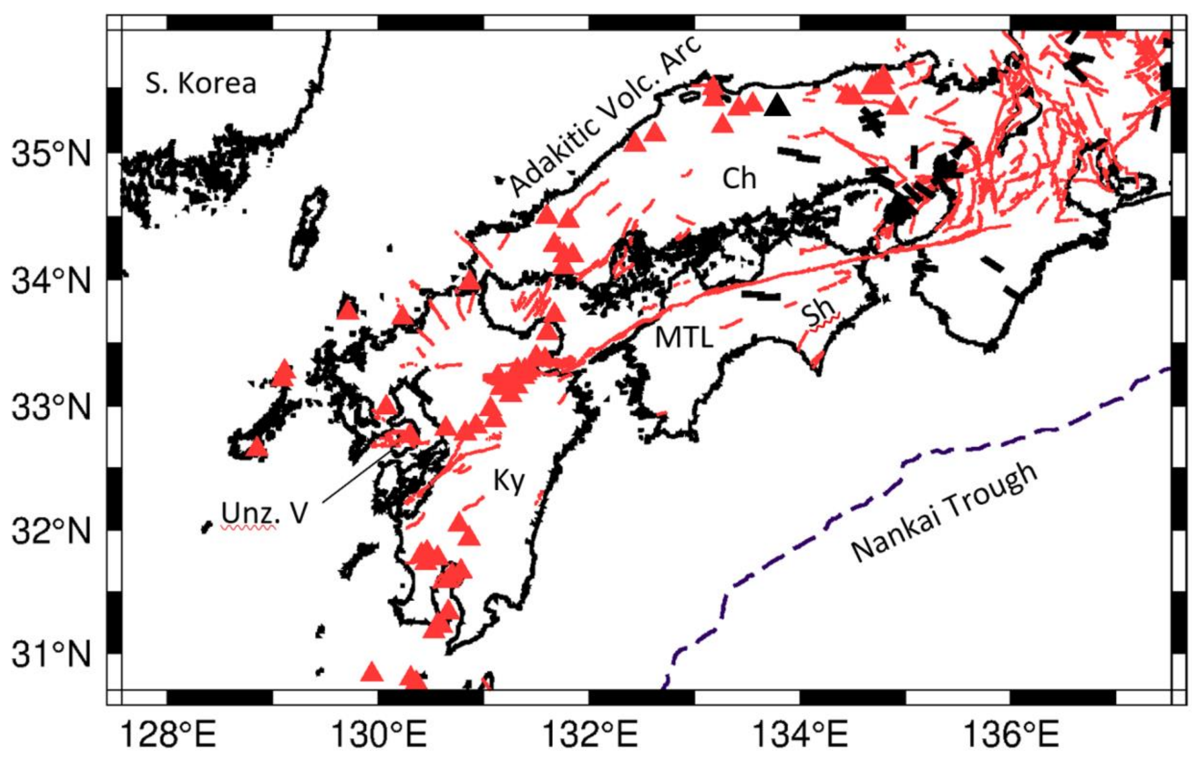

Figure 3. Tectonic map of southwest Japan. The red lines are active faults with the Median Tectonic Line abbreviated (MTL). The red triangles represent volcanoes. Black triangle marks the station used for analysis. The purple dashed line represents the Nankai Trough. The thick black lines represent crustal stress orientation. Chugoku, Shikoku, and Kyushu regions are abbreviated as Ch, Sh, and Ky, respectively. Map data is from the Active Fault Database of Japan (AIST)

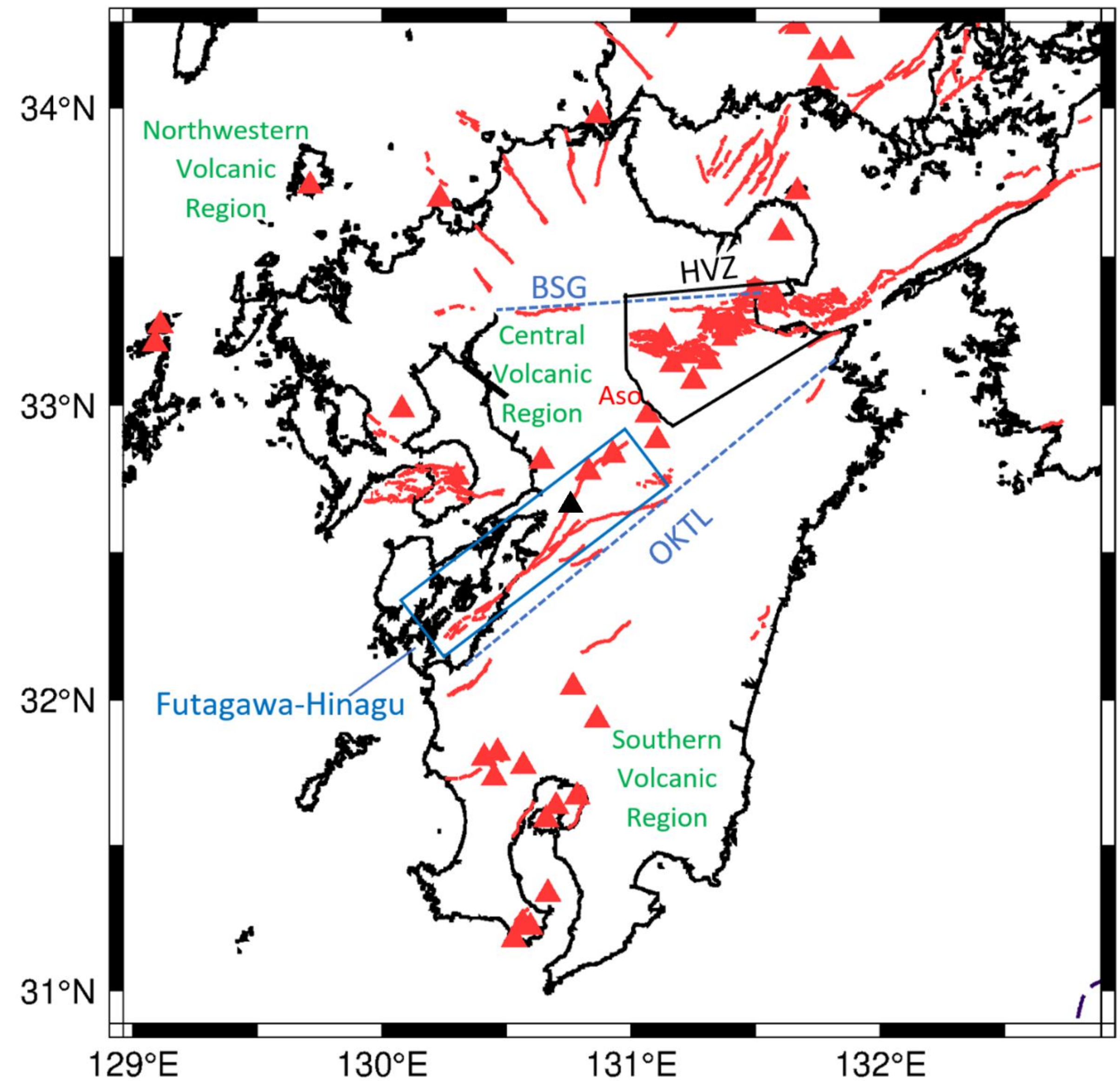

Figure 4. Tectonic map of Kyushu. Red lines represent active faults. Red triangles and red texts mark volcano locations. Black triangle marks the station used for analysis. Tectonic features have blue text; the dotted blue lines indicate the boundaries of the two grabens. Green texts represent the three volcanic regions. The blue box shows the Futagawa-Hinagu fault area. Thick black lines represent the volcanic zone. Abbreviations: BSG-Beppu-Shimabara graben; OKTL-Oita-Kumamoto tectonic line; HVZ-Hohi volcanic zone; Aso-Aso volcano. Map modified from Mahony et al. (2011). Fault and volcano locations are from the AIST

Kyushu lies at the junction of Southwest Japan and the Ryukyu Arcs (Fig. 4). The island has been under subduction of the Philippine Sea Plate ever since the late Miocene (Kamata and Kodama, 1994). During the late Miocene, N-S shortening deformation caused major back-arc folds, which initiated the transcurrent N-S Kokura-Tagawa Tectonic Line (KTL) (Itoh et al., 1992). Around 1-1.5 Ma, a convergence shift in a counterclockwise direction activated the transcurrent E-W Median Tectonic Line (MTL). Major active tectonic features in Kyushu are two strike-slip domains and two extensional grabens (Fig. 4). The Central Kyushu area is distributed with Plio-Pleistocene volcanic rocks, which form a volcano-tectonic depression, Hohi volcanic zone (HVZ) that is bounded by the KTL and MTL. The HVZ was created by N-S extension during the Quaternary, as evidence by the E-W trend of normal faults. The Beppu-Shimabara graben in central Kyushu reveals ongoing N-S extensional faulting (Kamata, 1994; Mahony, 2011). The extensional faulting coincides with abundant magmatic activity, extending southwest to back-arc rifting in the Okinawa Trough. The Oita-Kumamoto line is the Beppu-Shimabara extension graben's southern boundary, which consists of a system of dextral slip faults.

Chugoku lies to the north of Kyushu and Shikoku in southwest Japan (Figure 3). The tectonic structures in the inner zone of the western Chugoku are NE-trending reverse faults and fold. Chugoku has been seismically active with shallow seismicity aligned along a Quaternary adakitic volcanic arc 400 km from the trench (Morris, 1995; Gutscher, 1999) (Fig. 3). Flat subduction occurs along the Chugoku and Shikoku region due to the relatively young age of the Shikoku Basin lithosphere (Sacks, 1983). Seismic data in Chugoku also suggests that the slab beneath Chugoku has only reached 50-80 km depth. When the increased interplate coupling between two horizontal lithosphere causes upper plate deformation to move further inland, some of the transcurrent motion is transferred to the North Chugoku Shear Zone (NCSZ), whose seismic activity mimics the trend of the adakitic volcanic arc (Gutscher, 1999). Seismicity along the NCSZ can be quite high in the last century; the major fault has a history of deep low-frequency earthquakes and diverse earthquake activity (Gutscher, 1999).

2.1.2 Northeast Japan

In the Late Jurassic, northeast Japan was part of the Eurasia continent, with an accretionary prism forming at the eastern margin before the opening of the Japan Sea (Finn, 1994). It is known from surface geology that the Kuril arc collided with northeast Japan in the late Eocene to Oligocene. In the early Miocene, the opening of the Japan Sea separated Japan from the Eurasia continent (Jolivet et al., 1994). The region's brittle seismogenic zone was constrained within the upper 15 km of the crust of the Quaternary arc. Northeast Japan's substantial compressional tectonic stress supported by the upper crust resulted in the development of shallow thrust fault earthquakes (Hasegawa et al., 1978). The stress field of northeast Japan was extensional from 25 to 13 Ma, and it then changed to transitional from 13 Ma to 3.5 Ma. Around 3.5 Ma, the region's stress field changed to a crustal shortening stage by E-W compression (Sato, 1994) (Fig. 5). Off the coast of northeast Japan, the Pacific plate subducts beneath northeast Japan, which created the Japan Trench. Seismic and historical records show that large earthquakes of M $\geqslant$8.0 have occurred at the subduction zone (Lin et al., 2013).

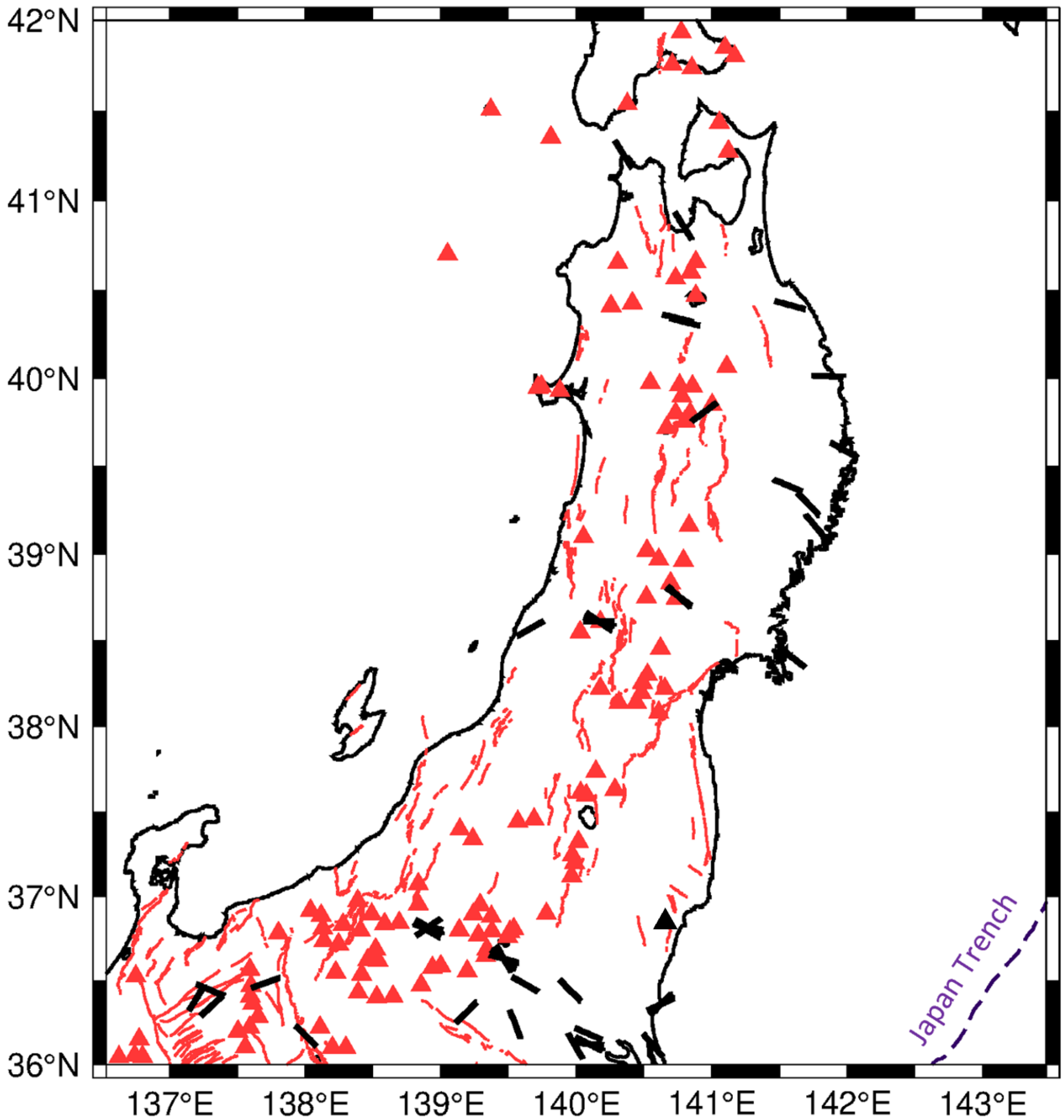

Figure 5. Tectonic map of northeast Japan. Red lines are active faults. Black triangle marks the station used for analysis. Black triangle marks the station used for analysis. Red triangles represent volcano locations. The purple dashed lines represent ocean trenches. Thick black lines indicate maximum horizontal stress directions. Map data is from the AIST.

2.1.3 Central Japan

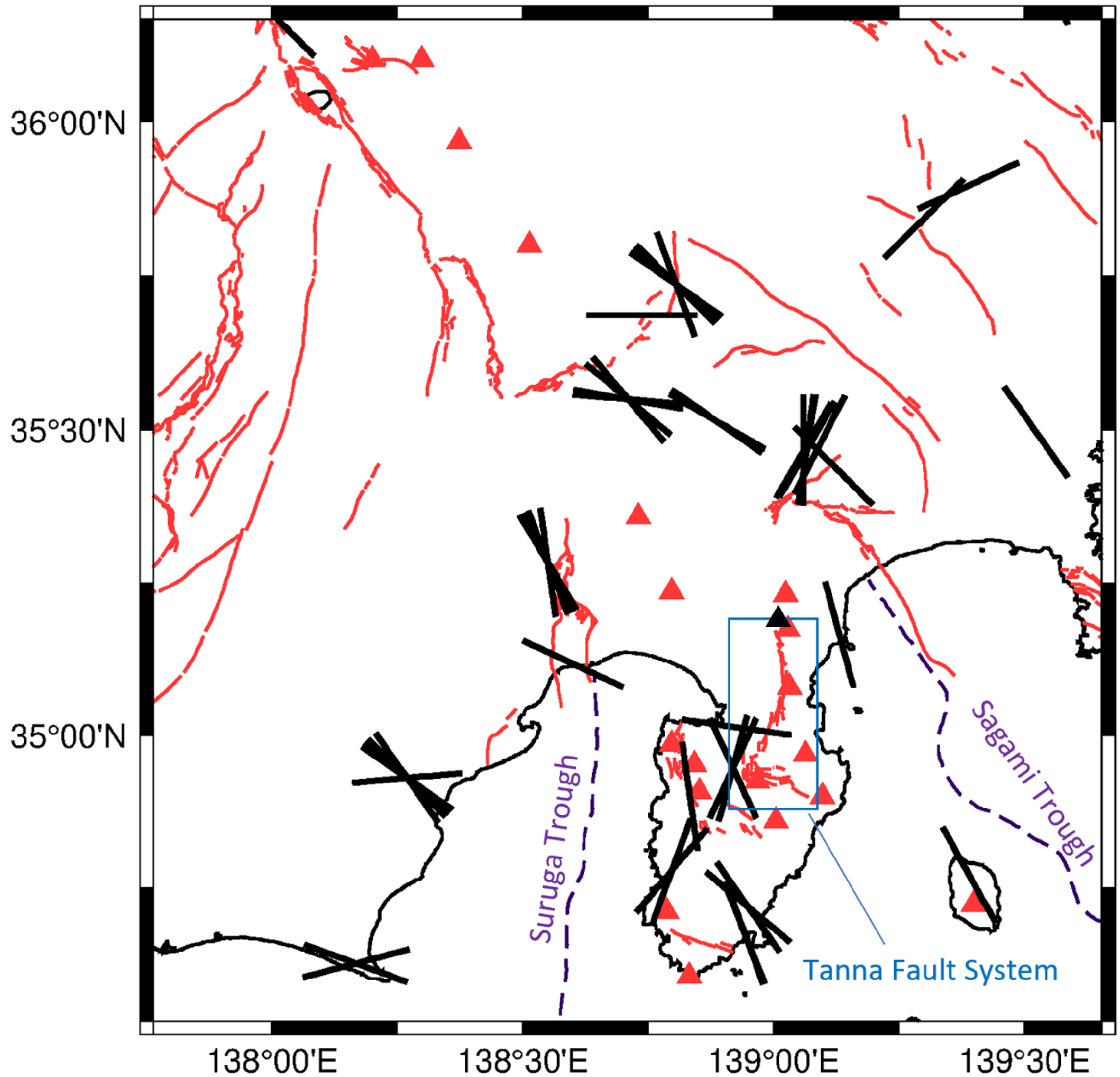

Figure 6. Tectonic map of the Tokai region in central Japan. Red lines are active faults. Red triangles represent volcano locations. Black triangle marks the station used for analysis. The purple dashed lines represent ocean trenches. Thick black lines indicate maximum horizontal stress directions. Blue box pinpoints the Tanna fault system. Fault and volcano locations are from the AIST.

The Tokai region is well-known for its seismic gap located southwest of Tokyo. In the Tokai region, the Philippine Sea Plate subducts beneath the continental plate at the Suruga Trough (Fig. 6), located northeast of the Nankai Trough. Due to the subduction of the Philippine Sea Plate, the Tokai area experiences large earthquakes offshore every 150 years. In the past 100 years, the Tokai region has been accumulating strain energy that can potentially result in an M_w 8 earthquake (Ozawa et al., 2016). The focal mechanisms of crustal earthquakes show an E-W compression axis except around the vicinity of the Suruga Trough (Saiga et al., 2003).

The Izu Peninsula is in the northern margin of the subducted Philippine Sea plate (Fig. 6). The subduction of the Philippine Sea plate beneath Honshu is deforming the Kita-Izu strike-slip fault system, which extends for as much as 35 km (Okubo et al., 1991). The Tanna fault is a N-S trending, left lateral fault, and it is the north fault of the Kita-Izu fault system. The Tanna fault is close to the Fuji volcanic zone, which produced and scattered young volcanic rocks around the fault. The Tanna fault zone consists of 24 fault strands with different strikes ranging from N-S, NNE-SSW, to E-W (Kimura et al., 2011).

2.2 Previous Studies

Observations on temporal changes in SWS have been documented in many publications (e.g., (Peacock et al., 1988; Crampin et al., 1990; Aster and Shearer, 1992; Li et al., 1994; Zhang and Schwartz, 1994; Munson et al., 1995; Crampin et al., 1999; Crampin, 2003; Saiga et al., 2003; Del Pezzo et al., 2004; Gao and Crampin, 2004; Hiramatsu et al., 2005; Bianco et al., 2006). Peacock et al., 1988 investigated SWS temporal variations at the Anza Seismic Gap, southern California, before the M_s 6 North Palm Springs earthquake. They identified temporal variations in delay time before a larger earthquake. They interpreted that the variations were due to the increase in crack aspect ratios in the distributions of stress-oriented fluid-filled microcracks as strain accumulated. The observations were further examined by other workers. Li et al. (1994) studied shear wave splitting at the Los Angeles Basin, and they observed stress-aligned shear wave splitting. However, their data were too sparse in time to show any significant temporal variations before several M5 earthquakes. Crampin and Gao (2005) later commented that there were enough earthquake data to support that time-delays did decrease immediately before the major earthquakes.

Crampin et al. (1999) claimed to successfully stress-forecast a major earthquake by observing variations in time delays of shear wave splitting in southwest Iceland. They reported that there was an increase in delay time several days before an M5 earthquake. The increase of delay time was interpreted as stress accumulation before large earthquakes. However, they noted that the stress forecast would require a substantial amount of seismic data or appropriate source-geophone geometry, which was challenging to meet. The increase in delay time was also observed 25 days before a mainshock in Italy (Del Pezzo et al., 2004) quake. Gao and Crampin (2004) later recognized that besides an increase in delay time before large earthquakes, there could also be a decrease in delay time immediately before a major earthquake. The decrease in delay time was associated with the merging of microcracks into larger cracks during the stress-accumulation (Gao and Crampin, 2006; Crampin et al., 2004; Crampin and Peacock, 2008).

Owing to Japan's dense seismic stations as well as its frequently occurring earthquakes, numerous studies in crustal anisotropy using SWS have been conducted in Japan and its vicinity (e.g., (Kaneshima et al., 1988; Kaneshima and Ando, 1989; Kaneshima, 1990; Saiga et al., 2003; Savage et al., 2016)). Kaneshima and Ando (1989) found that the fast polarization direction coincided with the tectonic stress in the Shikoku region of Japan and suggested that the seismic anisotropy was from the presence of vertical parallel cracks in the upper 15 km of the crust.

SWS analysis was also conducted in the Tokai region in central Japan (Saiga et al.,2003; Hiramatsu et al., 2005). Saiga et al. (2003) found that the delay time increased with focal depth down to 30 km, suggesting that regional compressive stress affects anisotropy in both the upper and lower crusts. They hypothesized that the temporal variations in time delays were caused by the changes in crack density and pore fluid pressure due to static stress change. However, there was no apparent precursory temporal change in time delay related to the main event (Saiga et al., 2003). Hiramatsu et al. (2005) revealed that the delay time for both crustal and slab source earthquakes increased and then decreased to the pre-event level over a period of 18 months. They concluded that the time delay variations after the earthquake were consistent with crack healing reported in laboratory experiments (Dieterich 1972; Dieterich 1978).

CHAPTER 3

DATA ANALYSIS

Data used in this study are three-component seismograms from earthquakes ($M_w \geqslant 1.0$) in Japan recorded by the high-sensitivity seismograph network (Hi-net) system that is operated by the National Research Institute for Earth Science and Disaster Resilience (NIED) (Fig. 7). First, we searched for mainshock events ($M_w \geqslant 6.0$) from the Hi-net database between January 1st, 2002, to August 1st, 2020. We found a total of eight mainshocks that are one month prior and within 50 km from the mainshocks. We tried to minimize the spatial distribution of the foreshocks from each other and the main events. The foreshocks should be in the same group of back azimuths as the mainshock. In addition, the number of foreshocks should be statistically sufficient for a nearby station to record. Thus, we narrowed down to four possible study areas (Fig. 7). We then gathered the data of foreshocks that occurred one month before each of the mainshocks. The number of events in our study area was around 600. Some stations had poor quality data that lack a component in the recorded seismograms due to unknown reasons.

Table 3.1 Chosen mainshocks in this study

Event Name	Origin Date & Time	Latitude	Longitude	Depth (km)
Fukushima	2011/04/11 17:16:12	36.946	140.673	6.4
Shizuoka	2011/03/15 22:31:46	35.309	138.714	1.9
Tottori	10/21/2016 14:07:23	35.38	133.856	10.6
Kumamoto	4/16/2016 1:25:05	32.755	130.763	12.4

We selected foreshocks that had good signal-noise ratios and epicentral distances within 20km from the stations. Events with distances larger than 20km did not satisfy the general requirements of the shear-wave window and were not included in our analyses. Magnitudes of the selected events were larger than M_w 1 to ensure a high signal-to-noise ratio (SNR) for good S-wave signals.

The data processing involved filtering three-component seismograms by a band-pass filter to suppress noises and enhance P and S-wave signals. Spectrum analyses from the data showed that high energy was recorded between 1 and 10 Hz. Thus, we used a band-pass filter of 1-5 and 1-8 Hz (Fig. 8). Other frequency bands were also applied when the signals from these two filters were not clear. Then, we rotated the vertical, N-S, and E-W (ZNE) components into ray-based components (LQT). The P-wave energy dominated the L component, Q was the radial component that contained SV energy, and T was the transverse component containing SH energy. The rotation maximized the S-wave energy on the Q and T components, thus enhancing the accuracy of SWS measurements (Yuan and Li, 2017).

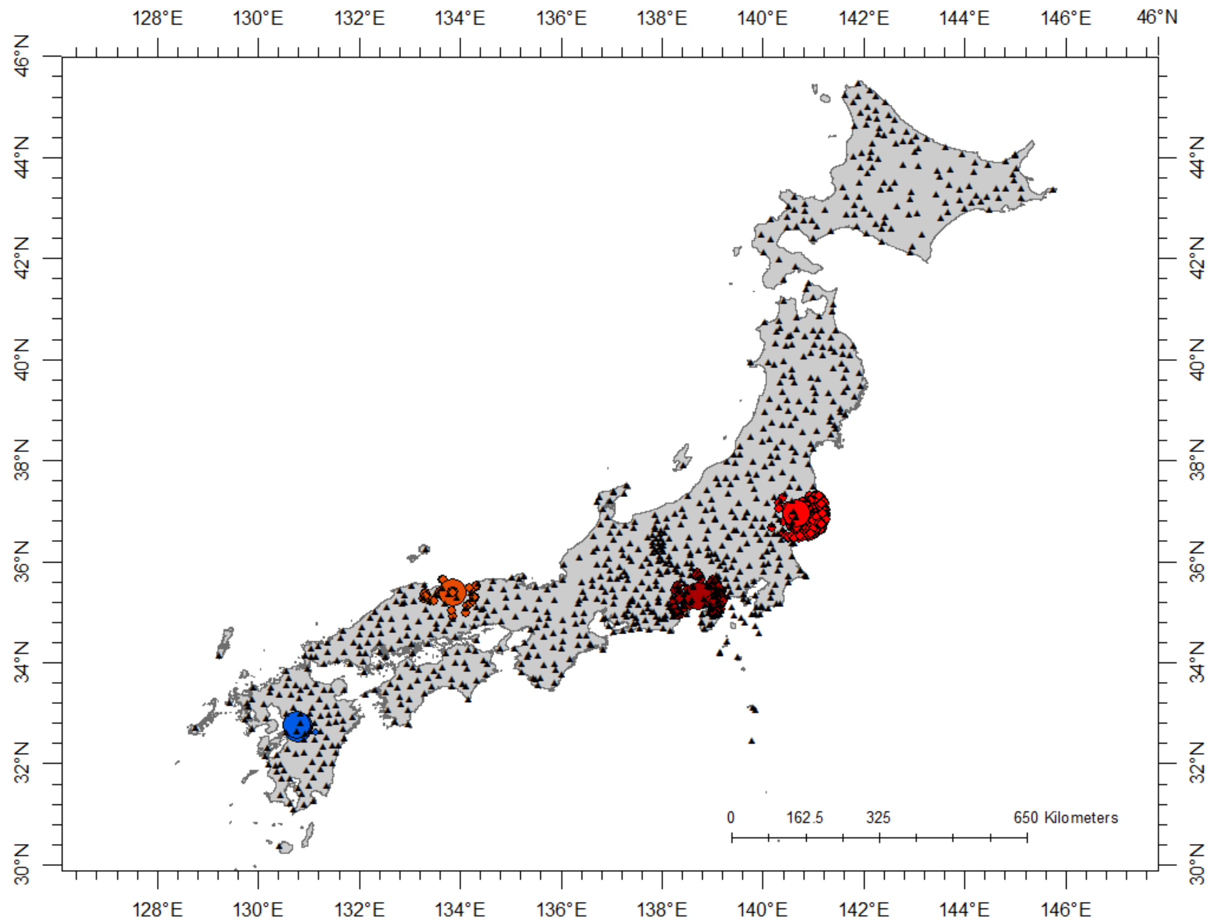

Figure 7. Map of foreshocks and mainshocks between January 1st, 2002, and August 1st, 2020. Black triangles represent the HiNet seismic stations. The earthquake magnitude correlates with the circle sizes.

a)

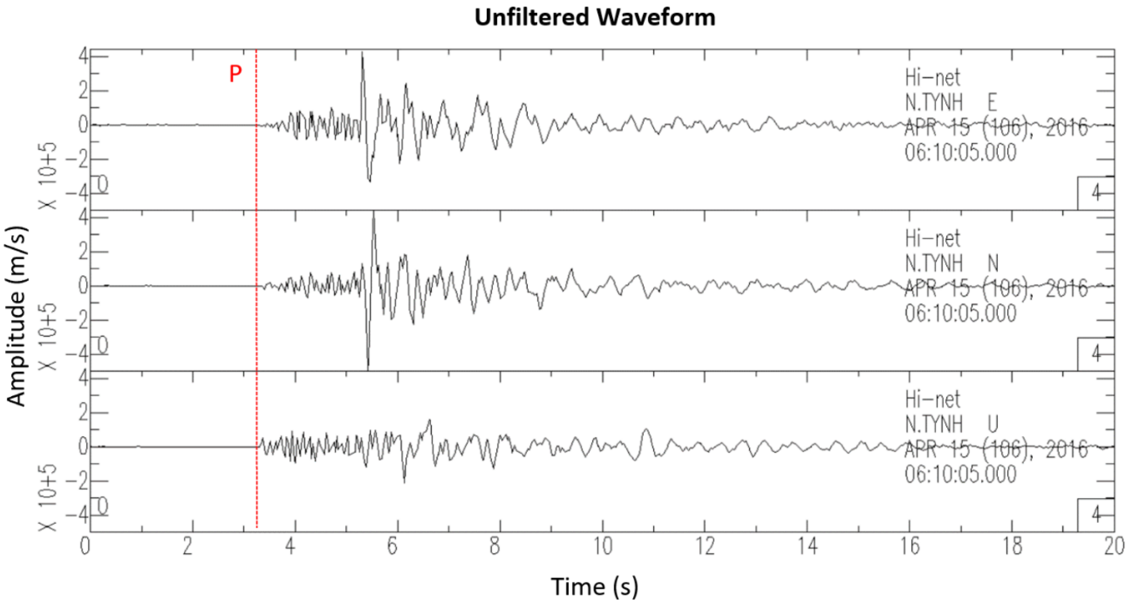

b)

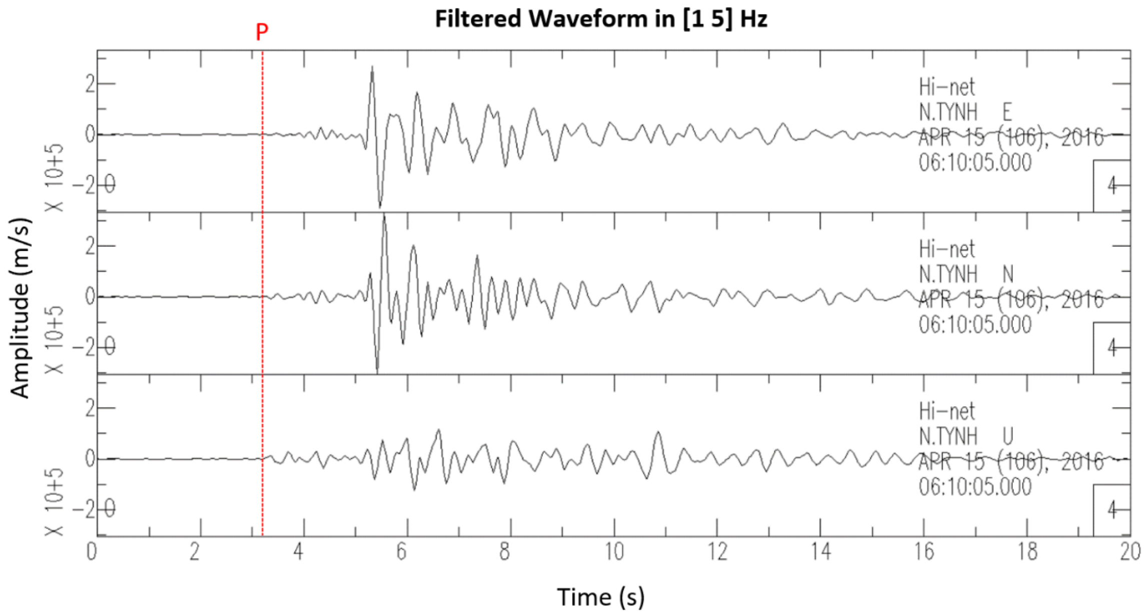

Figure 8. An example showing 3-component seismograms at station TYNH for event 2016-04-15 at the Kumamoto area. (a) Original seismograms of the ENZ components. (b) Filtered seismograms.

CHAPTER 4

METHODOLOGY

Splitting parameters are measured using several methods, such as the cross-correlation method, the transverse minimization method, and the eigenvalue method. The data used in all these methods are windowed seismograms containing S wave signals. The cross-correlation method uses two rotated and time-shifted orthogonal horizontal components to search for the maximum cross-correlation coefficient and return the splitting parameters (Fukao, 1984). The transverse minimization and the eigenvalue method search for the most singular covariance matrix of rotated and time-shifted seismograms (Silver and Chan, 1991). The difference between the transverse minimization and the eigenvalue method is that the eigenvalue method minimizes the smaller eigenvalue of the corrected matrix instead of minimizing the energy on the transverse component (Silver and Chan, 1991). In this study, we used the eigenvalue method to acquire the SWS measurements.

4.1 Eigenvalue Method

The eigenvalue value method, introduced by Silver and Chan (1991), uses an inverse splitting operator ($\Gamma^{-1}(\phi', \delta t')$) to reverse the splitting effects to retrieve the original wave before splitting. The splitting operator ($\Gamma(\phi, \delta t)$) rotates and time shifts an unsplit wave by $\pm\delta t/2$, which is defined by Silver and Chan as

$$\Gamma(\phi, \delta t) \equiv \exp(i\omega\delta t/2)\hat{\mathbf{f}}\hat{\mathbf{f}} + \exp(-i\omega\delta t/2)\hat{\mathbf{s}}\hat{\mathbf{s}} \qquad (4\text{-}1)$$

where ω represents the angular frequency, $\hat{\mathbf{f}}$ and $\hat{\mathbf{s}}$ are the fast and slow polarization directions of the polarization matrix V, defined by

$$\rho V_{il} \equiv c_{ijkl} b_j b_k \quad (4\text{-}2)$$

with ρ as density, V_{il} as polarization tensor, c_{ijkl} as the elastic coefficient, b_j and b_k are components of the propagation vector $\hat{\mathbf{b}}$.

We then performed a grid search over all possible pairs of fast direction (ϕ) and delay time (δt) by calculating the covariance matrix c_{ij} of the two orthogonal fast and slow components,

$$c_{ij}(\phi, \delta t) = \int_{-\infty}^{\infty} u_i(t) u_j(t - \delta t)\, dt \quad (4\text{-}3)$$

In isotropic cases, the covariance matrix will have one non-zero eigenvalue λ_1 while in anisotropic cases, $\boldsymbol{c}$ will have two non-zero eigenvalues $\lambda_1$and λ_2. The first eigenvalue λ_1 shows the particle motion after correcting for splitting. The optimal measurements are the pair of ($\phi, \delta t$) with the smallest 2nd eigenvalue and the most linear particle motion (Silver and Chan, 1991).

4.2 Estimating Errors

Once we identified the optimal pair of ϕ and δt, we estimated their standard deviations by calculating the half-width and length of the 95% confidence region. The confidence region is determined with the assumption that the sum of squares, which is constructed from ${\lambda_2}^{min}(\phi, \delta t)$, is approximately χ^2 distributed. The confidence region is calculated with ν degrees of freedom and k parameters as

$$\frac{\lambda_2}{\lambda_2^{min}} \leq 1 + \frac{k}{\nu - k} f_{k,\nu-k}(1 - \alpha) \quad (4\text{-}4)$$

where f is the inverse of the F-distribution, α is 0.05, k is the number of parameters, which is 2 ($\phi, \delta t$) in this case, and the product of ν and the sampling rate is usually equal to one degree of freedom (Silver and Chan, 1991).

4.3 Quality Control

We provided some quality control of the measured splitting parameters to ensure the reliability of the results. A splitting measurement is considered robust when it gives at least 0.9 linearities of the particle motion and has an error of δt less than 0.02s and an error of ϕ less than 20 degrees (Peng and Ben-Zion, 2004). An example of good SWS measurements is given in Figure 9. We also carefully checked the contour plots to remove possible cycle skipping measurements, which corresponded to a local minimum at a large delay time.

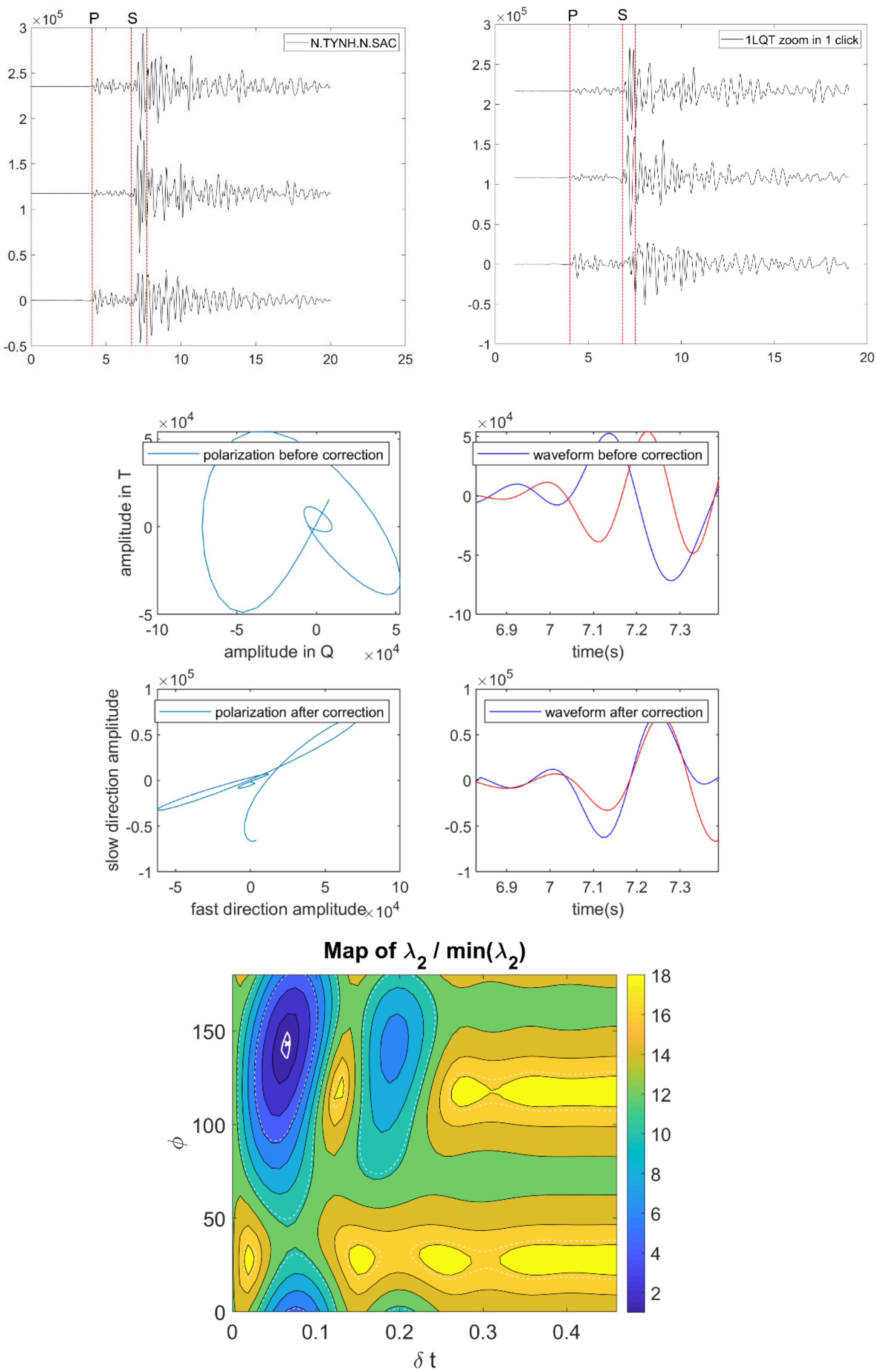

Figure 9. Example of a robust measurement. Notice the clean waveforms during picking, linear particle motion, matching waveforms after correction, and bulls-eye style contour plot.

CHAPTER 5

RESULTS

We utilized a semiauto algorithm in calculating SWS parameters based on the method of Silver and Chan (1991). The input data were filtered seismograms of the ENZ components. The incidence angle was calculated based on the P wave amplitude on each component, which was used to rotate the seismograms to the LQT components. SWS parameters $(\phi, \delta t)$ were estimated using the eigenvalue method (Silver and Chan, 1991) to the windowed S wave seismograms on the Q and T components. The algorithm also calculated a 95% confidence contour for the optimal measurements, which helped evaluate the quality of the measurements.

5.1 Overall SWS Measurements

We present all SWS measurements and the average for each station in four different areas in Figure 10 and Figure 11. The mean fast directions and delay times are also given in Table 5.1. The fast polarization directions of splitting shear waves from our results are consistent with previous studies. The fast directions are parallel to the maximum horizontal stress (Savage et al., 2010; Li and Peng, 2017) or parallel to fault strikes at stations close to active faults (Cochran et al., 2006). The fast directions at station SKGH at the Tottori area are consistently NW-SE, roughly agreeing with the nearby fault strike in the WNW-ESE direction (Figure 3). SWS measurements at Fukushima have diverse fast directions, with most of them in the NNE-SSW and the NNW-SSE directions. The average fast direction is in the NW-SE direction, inconsistent with the regional stress field, which is E-W (Figure 5) (Kaneshima, 1990). Nevertheless, our results agree with the fast directions from

Iidaka and Obara (2013), who measured SWS parameters at the same station (JUOH). The average fast direction (151^{o}) generally follows the Shinohara and Idosawa active faults strike, which is approximately N-S (Kobayashi et al., 2012).

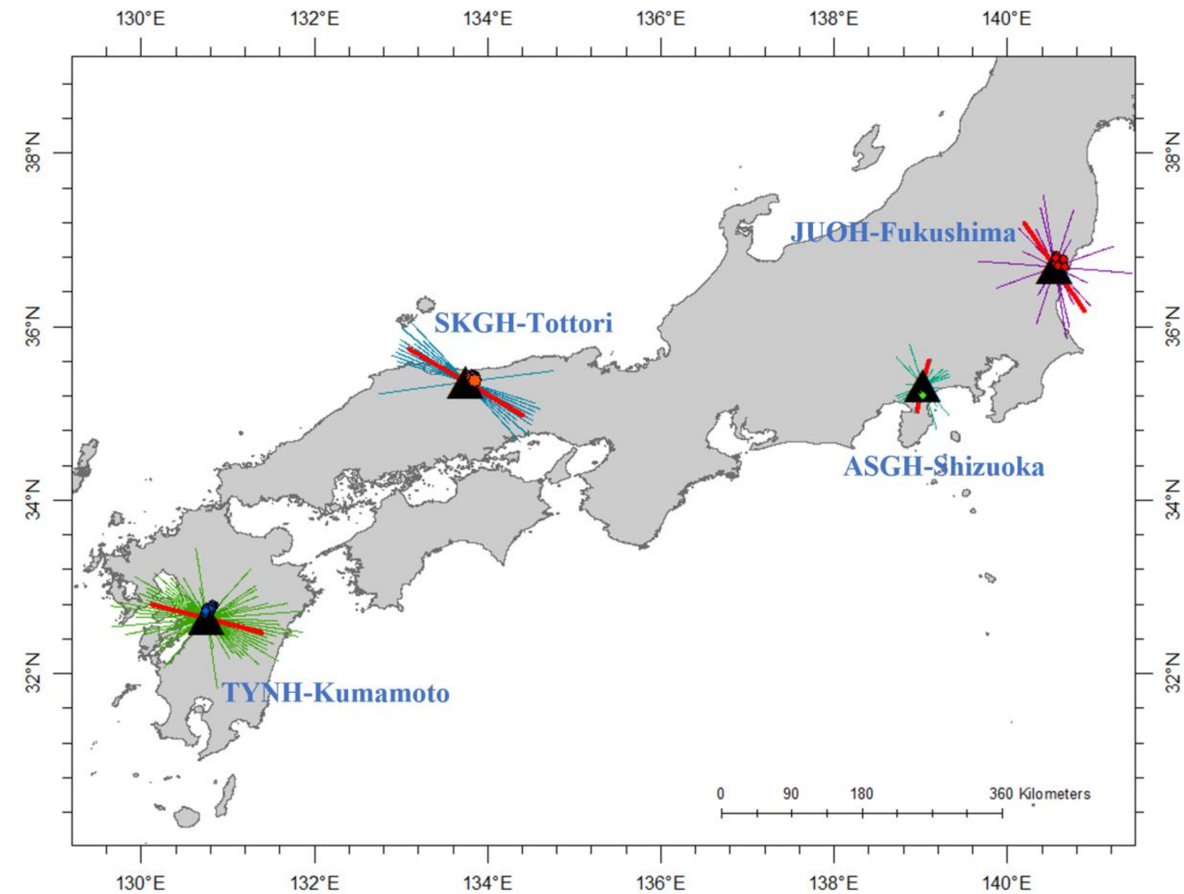

Figure 10. Selected shear wave splitting results for analysis. Black triangles represent the stations. The small circles show the events. The station and area names are located near each station. Each SWS result is plotted as one bar. The bars are parallel with the fast directions, and they are scaled with delay time. The thick red bars represent average SWS results at each station.

The observed fast polarization directions at station ASGH are complicated (Fig. 10 and Fig. 11b). The dominant fast direction is NE-SW, which does not correlate well with the regional maximum horizontal stress (Figure 6). The diverse fast directions could be due to the numerous fault strands striking in different directions in the Tanna fault zone (Kimura et al., 2011). At the Kumamoto area, the fast directions measured at the station TYNH are largely WNW-ESE (Fig. 10 and Fig. 11d), following the regional maximum horizontal stress. Our SWS measurements in Kumamoto agree with previous studies in this area (Kaneshima, 1990; Savage et al., 2016).

Table 5.1. Calculated average fast directions and delay time

Stations	Average fast direction ϕ (°)	Average delay time δt (s)
JUOH	151	0.07
ASGH	51	0.04
SKGH	122	0.09
TYNH	112	0.07

5.2 Spatial Variations

We plot SWS results at the event locations in Figure 11, helpful for evaluating lateral variations of crustal anisotropy. In the Fukushima area, the main event (7.0 M_w) (the large red dot) that occurred on April 11th, 2011, is an aftershock of the 2011 Tohoku earthquake (Fig. 11a). The foreshocks for this event distribute in a broad area, with different azimuths to station JUOH. The diverse fast directions at this station can be grouped based on the event locations. The fast direction from the three northernmost events is in NNE-SSW, while the fast directions from the events close to the station in the azimuths of NE are dominant in NNW-SSE. The different SWS measurements at station JUOH mostly reflect lateral heterogeneity of anisotropy, which could be due to complex fracture systems in the crust. SWS parameters at station ASGH are not consistent with different events even though they are located in a similar area (Fig. 11b), which must be due to other reasons instead of heterogeneity. At station SKGH, the events are in a narrow azimuth and the fast directions are consistently in NW-SE direction (Fig. 11c), indicating homogeneous anisotropy in this area. In the Kumamoto region, there are three large events ($M_w > 6$) (large blue dots) that occurred within 28 hours (Fig. 11d). The fast directions are dominantly NW-SE, consistent with the regional stress field in central Kyushu (Fig. 11d). The events further away from the station, to the north of the large events, give the approximately NW-SE fast directions, and the events closer to the station give almost E-W fast directions. The three large events lie on the same Hinagu fault but produce different anisotropy results. The varying fast directions could be due to the different ray paths, reflecting lateral heterogeneity in the anisotropic structure in the crust.

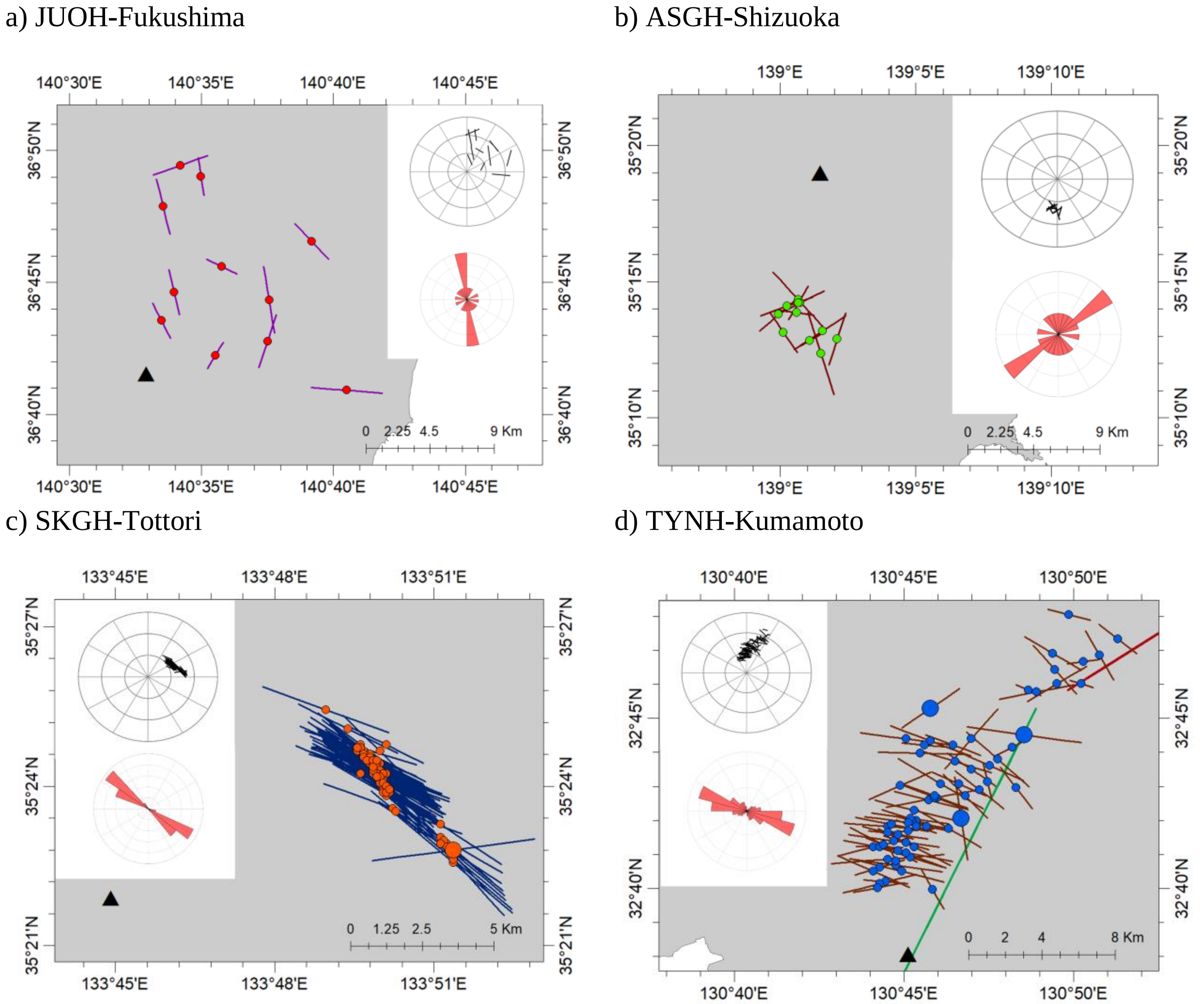

Figure 11. Spatial variations in four study areas. Black triangles show seismic stations. Small circles represent foreshocks. Big circles show events with $M_w \geqslant 6$. The rose diagram and equal area plots are for each station. The bars are scaled with delay time. The two thick lines in d represent major faults. Green-Hinagu; Red-Futagawa.

Temporal Variations

We plot the obtained delay times and fast directions as a function of time for each of the four areas in Figure 12 and Figure 13 to examine temporal variations of SWS parameters. There is no meaningful change in the delay time and fast direction at all four stations. Station ASGH lacks data within 48 hours before the mainshock, not a good data set for evaluating precursory anisotropy change. At station JUOH, there are two events within one day before the mainshock; their delay time appears to increase relative to the nearest foreshock around day five but is within the normal range for earlier foreshocks.

Station TYNH appears to be promising to evaluate temporal variations of delay time due to a large number of foreshocks. To avoid the effects of heterogeneity, we examine the delay time variations along the Hinagu fault (Green line in Fig. 11d) and plot the results in Fig. 12d. The delay time is heavily scattered for the Kumamoto area at station TYNH. The large range of delay times from 28 to 24 hours' time window at Kumamoto confirms that delay times from shear wave splitting measurements typically display a high scatter of approximately 80% (Crampin, 1999; Gerst and Savage, 2004). The scatter in delay time could be due to the rapid stress changes between each event (Crampin et al., 2004). We note a slight deviation in delay time from the mean within thirteen hours before the main event. Nevertheless, the amount of data within that time window is statistically insufficient to support a precursory increase before the major earthquake.

At station SKGH, the variation of delay time is small relative to the average value of 0.09 s. About a dozen events occurred within two hours before the mainshock; the fluctuation range of the delay times from these events is consistent with earlier foreshocks. However, there is a clear jump in the delay time from the average value of 0.08 s to 0.11 s around 86 minutes before the mainshock

(Figure 14). The average 0.11s is also larger than the long-term average of 0.09 s. These events are located in a similar area, eliminating the possible cause of heterogeneity. We also check the other two earthquake swarms at days 23 and 24 before the mainshock (Figure 14). The delay time from these two groups of events changes randomly around the average and does not show a sudden jump as for the latest foreshocks (Figure 14a). We also check the locations of close foreshocks (Figure 14d). The events associated with the smaller delay time are located relatively far to the north of the mainshock, while those with large delay times are very close to the mainshock. The sudden increase of delay time could be due to heterogeneity, at least partially, instead of a pure temporal variation. It does indicate that the area near the mainshock is more anisotropic.

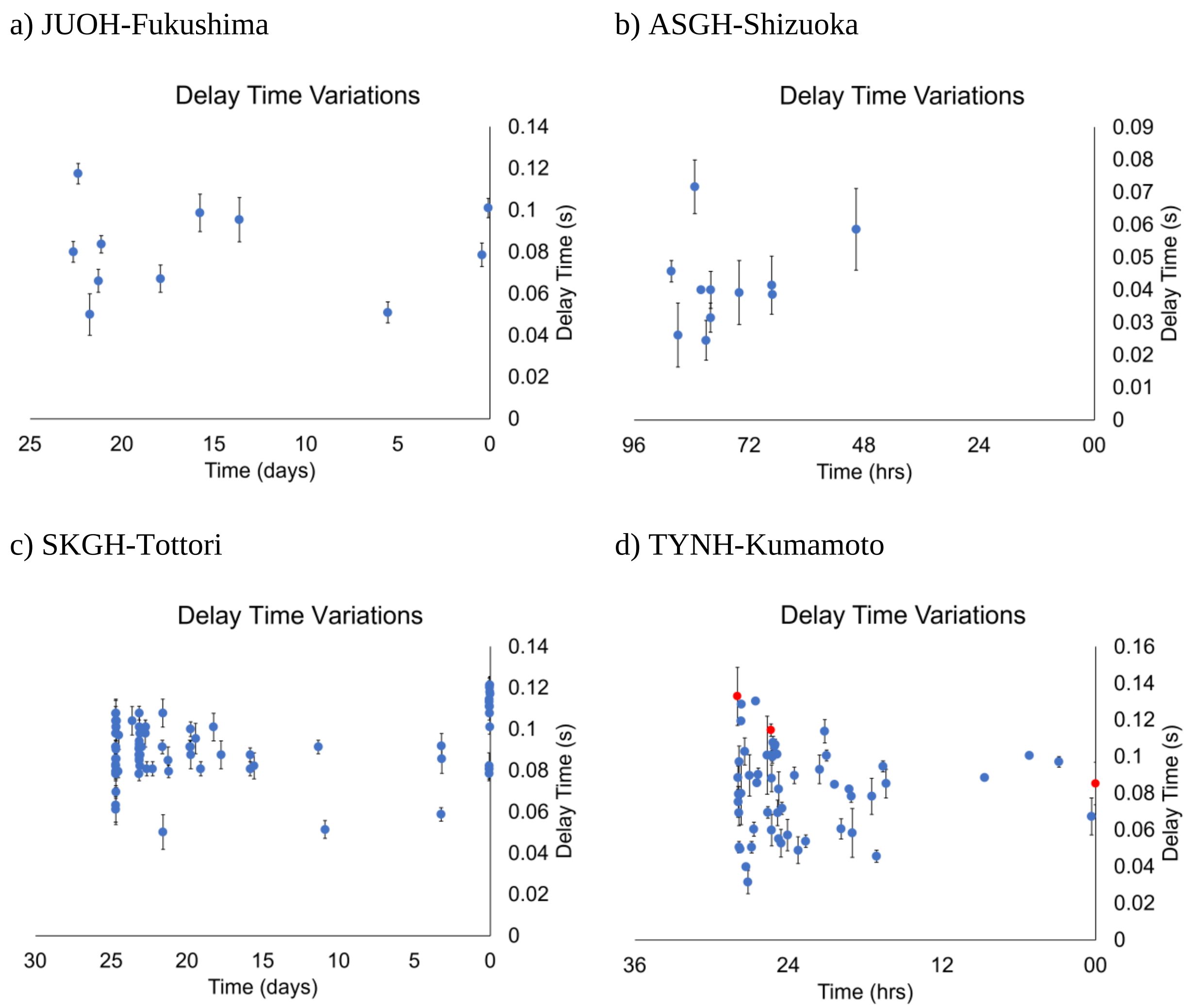

Figure 12. Delay time variations are plotted for different areas. The results at station TYNH are plotted for the events on the Hinagu fault only. The red circles indicate events with magnitudes larger than 6.

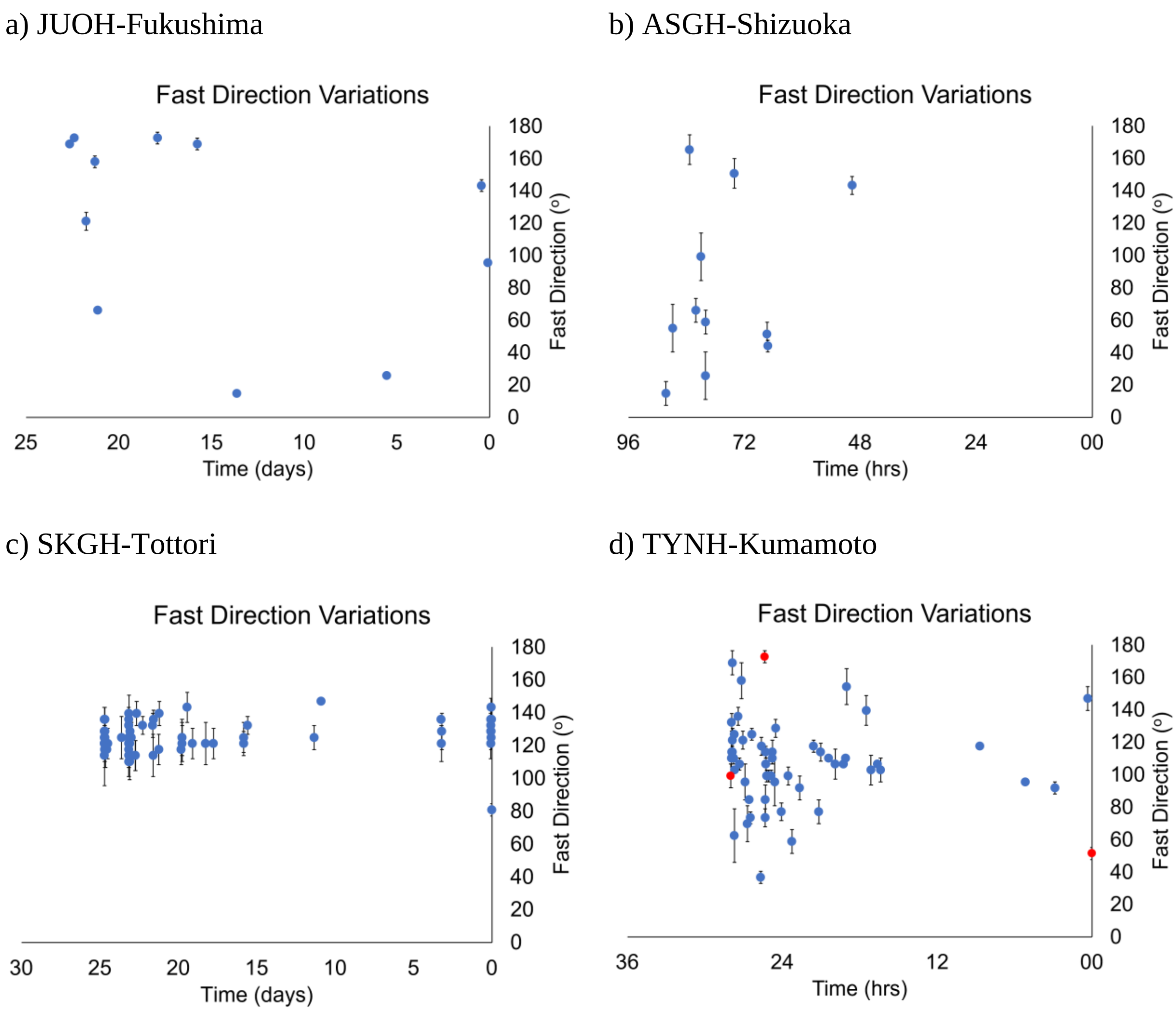

Figure 13. Fast direction variations are plotted for different areas. The results at station TYNH are plotted for the events on the Hinagu fault only. The red circles indicate events with magnitudes larger than 6.

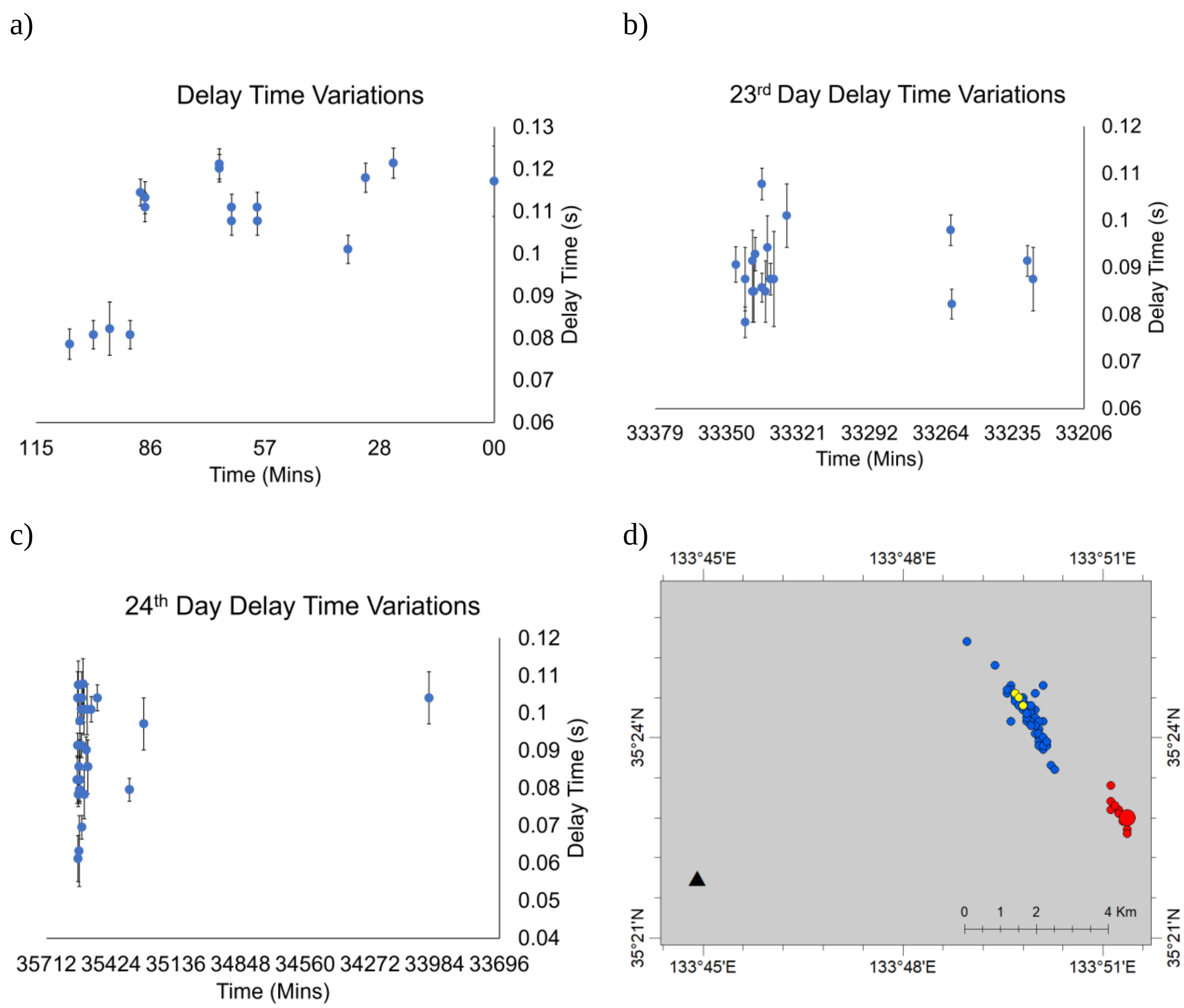

Figure 14. Details about temporal delay time variations and associated event distribution for station SKGH. (a) Delay times within two hours before the mainshock. (b) Delay times on the 23rd day before the mainshock. (c) Delay times on the 24th day before the mainshock. (d) The distribution of events associated with the delay times shown in (a). Yellow dots are for the four events with smaller delay times, and red dots are for the group of the latest foreshocks, which are closer to the mainshock (big red dot).

CHAPTER 6

DISCUSSION AND CONCLUSION

6.1 Discussion

We have analyzed seismic data and measured shear wave splitting parameters at four Hi-net stations in different parts of Japan. All four study seismic stations provide good earthquake swarm data with high-quality seismograms for shear-wave splitting analyses. The results are generally compatible with previous studies' findings in Japan (Iidaka and Obara, 2013; Kaneshima, 1990; Kimura et al., 2011; Savage et al., 2016). In general, the fast directions at all four stations are either parallel with the nearby geological structure or with the regional maximum horizontal stress. The fast polarization directions in the Fukushima and Kumamoto areas display variability with different groups of back azimuths. This suggests that the results depend on ray paths, indicating the presence of lateral heterogeneity in crustal anisotropy.

The temporal variations of delay time do not show a clear precursory increase or decrease prior to the main events except at station SKGH in Tottori. There are several factors affecting the success of observing precursory anisotropy change before major earthquakes. The most common reason is the lack of data. It could be that foreshocks are too sparse or too far from the mainshock, or there is no station close to the events. Even though the Hi-net stations are densely distributed across Japan, we are still limited by the number of stations that provide high-quality data for SWS analyses. The foreshocks are sparse in time at JUOH in Fukushima and at ASGH in Shizuoka. In Kumamoto, even though there are many events recorded by station TYNH, the first event in the group is already a major event with a magnitude larger than 6. Therefore, the other events can be considered as aftershocks of this first mainshock instead of foreshocks. It is not a surprise that the delay times at TYNH do not show a noticeable trend.

Delay times are affected by ray paths, which depend on the epicentral distance and source depth. Fig. 15 shows delay times versus distance and depth in all four areas. The delay times do not show any correlation with hypocentral depth and epicentral distance, suggesting that anisotropy is probably shallow in the uppermost few kilometers of the crust as proposed in previous studies (Shih and Meyer, 1990; Audoine et al., 2000; Graham et al., 2020). Therefore, only a small segment of ray paths samples the anisotropic medium. The average delay time is 0.07s at JUOH, 0.04s at ASGH, 0.09s at SKGH, 0.07s at TYNH. These small values of delay time also support that anisotropy is in the shallow crust. Otherwise, the delay time is expected to increase with source depth and epicentral distance. Saiga et al. (2003) observed consistent shear wave splitting results down to 30 km in the Tokai region. However, it is difficult to detect the exact depth range of anisotropy in this study since the events are not directly above the earthquakes, and the ray paths are similar for events in a small area.

Lateral heterogeneity of crustal anisotropy also affects the success of observing precursory delay time change. Even though there are enough foreshocks, if they are not from the same small cluster and there is lateral anisotropy variation, SWS parameters from these events could be different due to different ray paths, like the situations in Fukushima and Kumamoto (Figs. 11a and 11d). The increase of crack density before a large earthquake could concentrate in a narrow zone near the fault. If ray paths do not travel in this fracture zone or only travel in this zone for a short distance, the delay time is probably not much affected by this property change. If a source and a receiver align along the fault strike, the ray path travels a long distance in the fracture zone and may produce a large delay time. Nevertheless, measured delay times are also affected by the relation between the initial S-wave particle motion and the crack plane. If the particle motion is parallel or perpendicular to the crack plane, it results in a null measurement. The change in the angle between the particle motion and the crack plane also cause variations in delay time (Crampin et al., 1990). Thus, repeating earthquakes with similar mechanisms and locations are critical for observing precursory anisotropy changes.

The observation of a 0.03 s delay time jump within two hours before the mainshock in Tottori provides strong evidence for the increase of anisotropy strength near the source region before a large earthquake, supporting the theory of dilatancy (Brace et al., 1966, Scholz et al., 1973). However, the range experiencing dilatancy is probably small, which makes it difficult to observe the phenomena in real data. Despite the strict criteria required to use SWS to study precursory changes, the method can be combined with other techniques to elucidate the observed phenomena. For instance, variations in the V_p/V_s ratio can help indirectly identify fluid and crack migration within the crust (Nur, 1971). An increase in V_p/V_s ratio may indicate an increase in pore fluid pressure; thereby, the technique can help to clarify SWS observations. Although there are some limitations on foreshock data and available receivers, the SWS method is simple and effective in observing precursory anisotropy when there are good foreshock data. Additional studies using the SWS method to study foreshocks before other major earthquakes are needed to verify the presence of precursory anisotropy, which could have a great impact on forecasting large earthquakes.

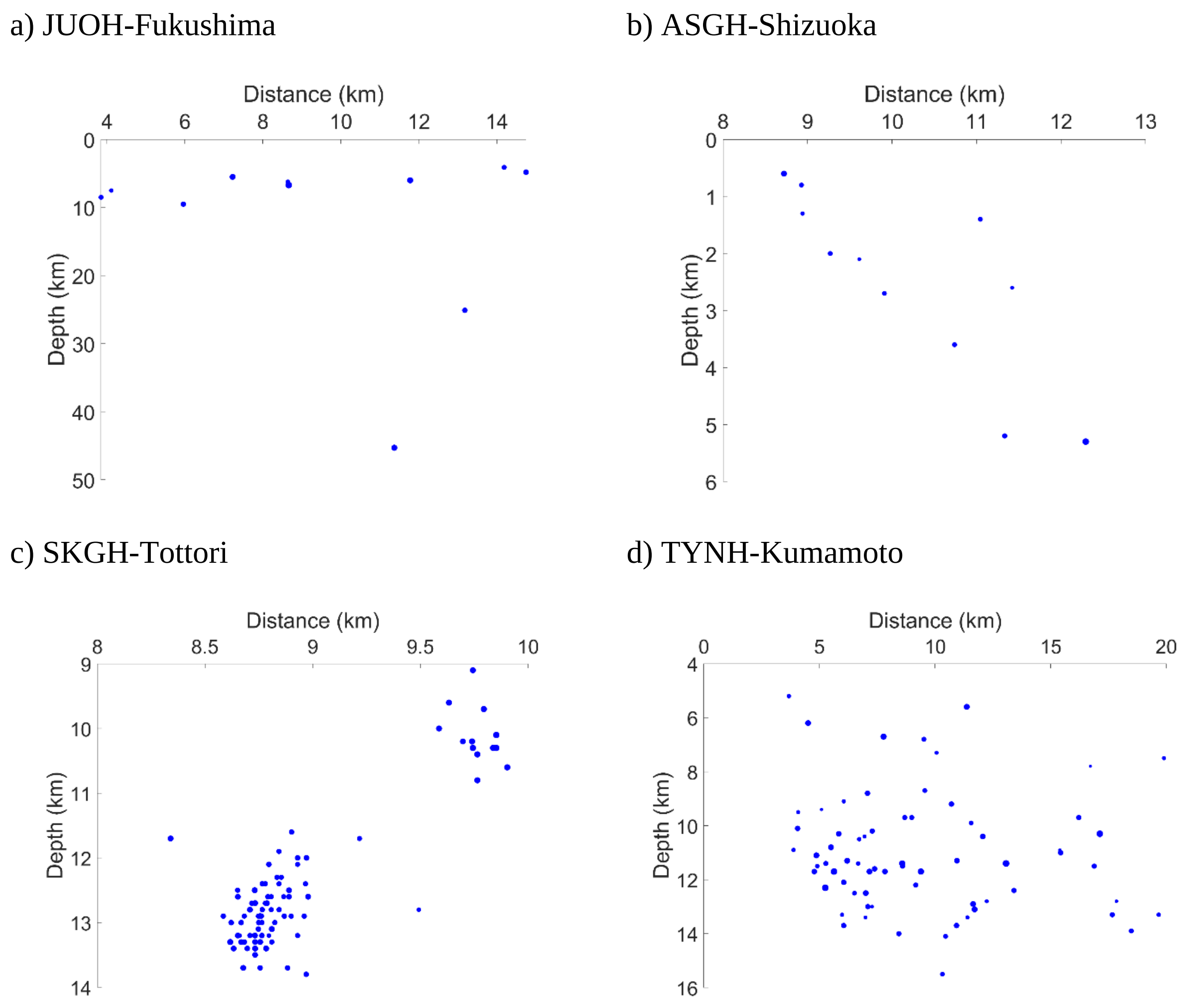

Figure 15. Variations of shear wave splitting delay times with epicentral distances and depths in four areas. The circle size is scaled by delay time.

6.2 Conclusion

We have measured SWS parameters from foreshocks before several major earthquakes in Japan. The fast directions at four stations in different areas agree with nearby geological structures and regional maximum horizontal stress. We also find that the fast direction varies with back azimuth, which is clearly evident at station JUOH in Fukushima and at TYNH in Kumamoto due to a broad event back azimuth range. Anisotropy changes associated with significantly different ray paths could be caused by lateral heterogeneous anisotropy instead of temporal variations. The delay times in all areas do not depend on epicentral distance or event depth, suggesting that anisotropy is largely confined in the upper few kilometers.

The delay times do not show any clear temporal variation over the one month of foreshocks data. Station JUOH in Fukushima and ASGH in Shizuoka have too few foreshock events closely before the mainshocks, hindering the detection of any precursory anisotropy phenomenon. Three large events are in the data set at station TYNH in Kumamoto. Therefore, the foreshocks before the late major event are also aftershocks of the earlier ones, and they are not good for observing precursory anisotropy. The only remarkable temporal change in delay time is a 0.03 s jump within two hours before the major earthquake in Tottori recorded at station SKGH. This change is not obvious in the plot with one-month data but robust at the short time window of two hours. The sudden change is between two groups of events. The earlier group is relatively far from the mainshock, and the latter group is immediately near the mainshock, evidencing that dilatancy before a major earthquake is limited in a small nucleation region. The absence of delay time increases in earlier foreshocks suggests that dilatancy exists in a short time before the large fault rupture. This limitation in time and space of dilatancy makes it extremely difficult to observe precursory anisotropy changes. This challenging task is still possible when favorable foreshock datasets are recorded.

BIBLIOGRAPHY

Aster, R. C., Shearer, P. M., 1990. Quantitative measurements of shear wave polarizations at the Anza Seismic Network, southern California: Implications for shear wave splitting and earthquake prediction. Journal of Geophysical Research, vol. 95, no. B8, p. 12449-12473.

Aster, R. C., Shearer, P. M., 1992. Initial shear wave particle motions and stress constraints at the Anza Seismic Network. Geophysical Journal International, vol. 108, p. 740-748.

Audoine, E., Savage, M. K., Gledhill, K., 2000. Seismic anisotropy from local earthquakes in the transition region from a subduction to a strike-slip plate boundary, New Zealand. Journal of Geophysical Research: Solid Earth, vol. 105, p. 8013-8033.

Barber, A. J., 1982. Interpretations of the tectonic evolution of Southwest Japan. Proceedings of the Geologists Association, v. 93, p. 131-145.

Bianco, F., Scarfi, L., Pezzo, D. E., Patane, D., 2006. Shear wave splitting changes associated with the 2001 volcanic eruption on Mt. Etna. Geophysical Journal International, vol. 167, p. 959-967.

Booth, D. C., Crampin, S., Lovell, J. H., Chiu, J. M., 1990. Temporal changes in shear-wave splitting during an earthquake swarm in Arkansas. Journal of Geophysical Research, vol. 95, p. 11151-11164.

Brace, W. F., Paulding, B. W., Scholz, C., 1966. Dilatancy in the fracture of the crystalline rocks. Journal of Geophysical Research, vol. 71, no. 16, p. 3939-3953.

Cochran, E. S., Li, Y. G., Vidale, J. E., 2006. Anisotropy in the shallow crust observed around the San Andreas Fault before and after the 20044 M 6.0 Parkfield earthquake. Bulletin of the Seismological Society of America, vol. 96, p. 364-375.

Crampin, S., Evan, R., Atkinson, B. K., 1984. Earthquake prediction: a new physical basis. Geophysical Journal International, vol. 76, p. 147-156.

Crampin, S., Booth, C. D., Evans, R., Peacock, S., Fletcher, B. J., 1990. Changes in shear wave splitting at Anza near the time of the North Palm Springs Earthquake. Journal of Geophysical Research: Solid Earth, v. 95, no. B7, p. 11197-11212.

Crampin, S., Volti, T., Stefansson, R., 1999. A successfully stress-forecast earthquake. Geophysical Journal International, v. 138, p. F1-F5.

Crampin, S., 2003. The New Geophysics: shear-wave splitting provides a window into the crack-critical rock mass. Leading Edge, vol. 22, p. 536-549.

Crampin, S., Peacock, S., Gao, Y., Chastin, S., 2004. The scatter of time-delays in shear-wave splitting above small earthquakes. Geophysical Journal International, v. 156, p. 39-44.

Crampin, S., Peacock, S., 2008. A review of the current understanding of seismic shear-wave splitting in the Earth's crust and common fallacies in interpretation. Wave Motion, v. 45, p. 675-722.

Dieterich, J. H., 1972. Time-dependent friction in rocks. Journal of Geophysical Research, vol. 77, p. 3690-3697.

Dieterich, J. H., 1978. Preseismic fault slip and earthquake prediction. Journal of Geophysical Research, vol. 83, no. B8, p. 3941-3948.

Finn, C., Kimura, G., Suyehiro, K., 1994. Introduction to the special section Northeast Japan: A case history of subduction. Journal of Geophysical Research, v. 99, no. B11, p. 22137-22145.

Fukao, Y., 1984. Evidence from core-reflected shear waves for anisotropy in the Earth's mantle. Nature, vol. 309, p. 695-698.

Gao, Y., Crampin, S., 2004. Observations of stress relaxation before earthquakes. Geophysical Journal International, v. 157, p. 578-582.

Gao, Y., Crampin, S., 2006. A further stress-forecast earthquake (with hindsight), where migration of source earthquakes causes anomalies in shear-wave polarizations. Tectonophysics, v. 426, p. 253-262.

Gerst, A., Savage, M., 2004. Seismic anisotropy beneath Ruapehu volcano: a possible eruption forecasting tool. Science, vol. 306, p. 1543-1547.

Graham, K, M., Savage, M, K., Arnold, R., Zal, H, J., Okada, T., Iio, Y., Matsumoto, S., 2020. Spatio-temporal analysis of seismic anisotropy associated with the Cook Strait and Kaikoura earthquake sequences in New Zealand. Geophysical Journal International, vol. 223, p. 1987-2008.

Gutscher, L., 1999. Birth of a major strike-slip fault in SW Japan. Terra Nova, vol. 11, p. 203-209.

Hiramatsu, Y., Honma, H., Saiga, A., Furumoto, M., Ooida, T., 2005. Seismological evidence on characteristic time of crack healing in the shallow crust. Geophysics Research Letter, v. 32.

Hasegawa, A., Umino, N., Takagi, A., 1978. Double-planed structure of the deep seismic zone in the northeastern Japan arc. Tectonophysics, vol. 47, p. 43-58.

Iidaka, T., Obara, K., 2013. Shear-wave splitting in a region with newly-activated seismicity after the 2011 Tohoku earthquake. Earth, Planets and Space, vol. 65, p. 1059-1064.

Iio, Y., 1996. Depth-dependent change in the focal mechanism of shallow earthquakes-Implications for brittle-plastic transition in a seismogenic region. Journal of Geophysical Research, v. 101, no. B5, p. 11209-11216.

Isozaki et al., 2011. Growth and shrinkage of an active continental margin: Updated Geotectonic History of the Japanese Islands. Journal of Geography, v. 120, p. 65-99.

Itoh, Y., Takemura, K., Kamata, H., 1998. History of basin formation and tectonic evolution at the termination of a large transcurrent fault system – deformation mode of central Kyushu, Japan. Tectonophysics, v. 284, p. 135-150.

Jolivet, L., Tamaki, K., Fournier, M., 1994. Japan Sea, opening history and mechanism: A synthesis. Journal of Geophysical Research: Solid Earth, American Geophysical Union, v. 99, no. B11, p. 22237-22259.

Kamata, H., Kodama, K., 1994. Tectonics of an arc-arc junction an example from Kyushu Island at the junction of the Southwest Japan Arc and the Ryukyu Arc. Tectonophysics, v. 233, p. 69-81.

Kamata, H., Kodama, K., 1999. Volcanic history and tectonics of the Southwest Japan Arc. The Island Arc, v. 8, p. 393-403.

Kamiyama, M., Sugito, M., Kuse, M., Schekotov, A., Hayakawa, M., 2016. On the precursors to the 2011 Tohoku earthquake: crustal movements and electromagnetic signatures. Geomatics, Natural Hazards and Risk, vol. 7, p. 471-492.

Kaneshima, S., Ito, H., Sugihara, M., 1988. Shear-wave splitting observed above small earthquakes in a geothermal area of Japan. Geophysical Journal, vol. 94, p. 399-411.

Kaneshima, S., Ando, M., 1989. An analysis of split shear waves observed above crustal and uppermost mantle earthquakes beneath Shikoku, Japan: Implications in effective depth extent of seismic anisotropy. Journal of Geophysical Research: Solid Earth, vol. 94, p. 14077-14092.

Kaneshima, S., 1990. Origin of crustal anisotropy-Shear wave splitting studies in Japan. Journal of Geophysical Research, v. 95, no. B7, p. 11121-11133.

Kato, A., Fukuda, J., Nakagawa, S., Obara, K., 2016. Foreshock migration preceding the 2016 Mw 7.0 Kumamoto earthquake, Japan. Geophysical Research Letters, vol. 43, p. 8945-8953.

Kimura, H., Ishikawa, N., Sato, H., 2011. Estimation of total lateral displacement including strike–slip offset and broader drag deformation on an active fault: Tectonic geomorphic and paleomagnetic evidence on the Tanna fault zone in central Japan. Tectonophysics, vol 501, p. 87-97.

Kobayashi, T., Tobita, M., Koarai, M., Okatani, T., Suzuki, A., Noguchi, Y., Yamanaka, M., Miyahara, B., 2012. InSAR-derived crustal deformation and fault models of normal faulting earthquake (Mj 7.0) in the Fukushima-Hamadori area. Earth, Planets and Space, vol. 64, p. 1209-1221.

Li, Y. G., Teng, T. L., Henyey, T. L., 1994. Shear-wave splitting observations in the northern Los Angeles basin, Southern California. Bulletin of the Seismological Society of America, vol. 84, p. 307-323.

Li, Z., Peng, Z., 2017. Stress- and Structure-Induced Anisotropy in Southern California From Two Decades of Shear Wave Splitting Measurements. Geophysical Research Letters, vol. 44, p. 9607-9614.

Lin, W., Conin, M., Moore, C. J., Chester, M. F., Nakamura, Y., Mori, J. J., Anderson, L., Brodsky, E. E., Eguchi, N., 2013. Stress state in the largest displacement area of the Tohoku-Oki Earthquake. Science, v. 339, p. 687-690.

Mahony, S. H., Wallace, L. M., Miyoshi, M., Villamor, P., Sparks, R. S. J., Hasenaka, T., 2011. Volcano-tectonic interactions during rapid plate-boundary evolution in the Kyushu region, SW Japan. Geological Society of America, v. 123, no. 11/12, p. 2201-2223.

Matsumoto, S., Nakao, S., Ohkura, T., Miyazaki, M., Shimizu, H., Abe, Y., Inoue, H., Nakamoto, M., Yoshikawa, S., Yamashita, Y., 2015. Spatial heterogeneities in tectonic stress in Kyushu, Japan and their relation to a major shear zone. Earth, Planets and Space, vol. 67, p. 172.

Morris, P. A., 1995. Slab melting as an explanation of Quaternary volcanism and aseismicity in southwest Japan. Geology, vol. 23, p. 395-398.

Munson, C. G., Thurber, C. H., Li, Y., Okuba, P. G., 1995. Crustal shear wave anisotropy in southern Hawaii: spatial and temporal analysis. Journal of Geophysical Research, vol. 99, p. 20367-20377.

Nakamura, K., Renard, V., Angelier, J., Azema, Z., Bourgois, J., Deplus, C., Fujioka, K., Hamano, Y., Huchon, P., Kinoshita, H., Laboume, P., Ogawa, Y., Seno, T., Takeuchi, A., Tanahashi, M., Uchiyama, A., Vignersse, J. L., 1987. Oblique and near collision subduction, Sagami and Suruga Troughs – preliminary results of the French-Japanese 1984 Kaiko cruise, Leg 2. Earth Planet. Sci. Lett, v. 83, p. 229-242.

National Institute of Advanced Industrial Science and Technology., 2012. Active Fault Database of Japan, February 28th, 2012 version. Research Information Database DB095, National Institute of Advanced Industrial Science and Technology.

National Research Institute for Earth Science and Disaster Resilience (2019), NIED Hi-net, National Research Institute for Earth Science and Disaster Resilience.

Nur, A., 1971. Effects of stress on velocity anisotropy in rocks with cracks. Journal of Geophysical Research, vol. 76, p. 2022-2034.

Okamura, Y., 2016. Active tectonics around the junction of Southwest Japan and Ryukyu arcs-control by subducting plate geometry and pre-Quaternary geologic structure. The Island Arc, v. 25, p. 287-297.

Okubo, Y., Mizugaki, K., Kanaya, H., 1991. Ground magnetic anomalies in the Tanna Fault and their implications. Journal of Geomagnetism and Geoelectricity, v. 43, p. 741-754.

Ozawa, S., Tobita, M., Yarai, H., 2016. A possible restart of an interpolate slow slip adjacent to the Tokai seismic gap in Japan. Earth, Planets and Space, vol. 68, p. 54.

Peacock, S., Crampin, S., Booth, C. D., 1988. Shear wave splitting in the Anza seismic gap, Southern California: Temporal variations as possible precursors. Journal of Geophysical Research, v. 93, no. B4, p. 3339-3356.

Peng, Z., Ben-Zion, Y., 2004. Systematic analysis of crustal anisotropy along the Karadere-Duzce branch of the North Anatolian fault. Geophysical Journal International, vol. 159, p. 253-274.

Pezzo, D. E., Bianco, F., Petrosino, S., Saccorotti, G., 2004. Changes in the coda decay rate and shear-wave splitting parameters associated with seismic swarms at Mt. Vesuvius, Italy. Bulletin of the Seismological Society of America, vol. 94, no. 2, p. 439-452.

Pritchard, M. E., Allen, R. M., Becker, T. W., Behn, M. D., Brodsky, E. E., Burgmann, R., Ebinger, C., Freymueller, J. T., Gerstenberger, M., Haines, B., Kaneko, Y., Jacobsen, S. D., Lindsey, N., McGuire, J. J., Page, M., Sergio, R., Tolstoy, M., Wallace, L., Walter, W. R., Wilcock, W., Vincent, H., 2020. New opportunities to study earthquake precursors. Seismological Research Letters, vol. 91, p. 2444-2447.

Sacks, I.S., 1983. The subduction of young lithosphere. Journal of Geophysical Research, vol. 88, p. 3355-3366.

Saiga, A., Hiramatsu, Y., Ooida, T., Yamaoka, K., 2003. Spatial variation in the crustal anisotropy and its temporal variation associated with a moderate-sized earthquake in the Tokai region, central Japan. Geophysical Journal International, vol. 154, p. 695-705.

Savage, M. K., Aoki, Y., Unglert, K., Ohkura, T., Umakoshi, K., Shimizu, H., Iguchi, M., Tameguri, T., Ohminato, T., Mori, J., 2016. Stress, strain rate and anisotropy in Kyushu, Japan. Earth and Planetary Science Letters, v. 439, p. 129-142.

Savage, M. K., Wessel, A., Teanby, N. A., Hurst, A. W., 2010. Automatic measurement of shear wave splitting and applications to time varying anisotropy at Mount Ruapehu volcano, New Zealand. Journal of Geophysical Research, vol. 115, no. B12321.

Scholz, C. H., Sykes, L. R., Aggarwal, Y. P., 1973. Earthquake prediction: a physical basis. Science, vol. 181, p. 803-810.

Shih, X. R., Meyer, R. P., 1990. Observation of shear wave splitting from natural events: South moat of long valley caldera, California, June 29th to August 12th, 1982. Journal of Geophysical Research: Solid Earth, vol. 95, p. 11179-11195.

Silver, P. G., Chan, W. W., 1991. Shear wave splitting and subcontinental mantle deformation. Journal of Geophysical Research, vol. 96, no. B10, p. 16429-16454.

Taira, A., 2011. Tectonic evolution of the Japanese Island Arc System. Annual Reviews Earth Planet Sciences, v. 29, p. 109-34.

Townend, J., Zoback, M. D., 2006. Stress, strain and mountain building in central Japan. Journal of Geophysical Research, vol. 111, no. B03411.

Wang, Z., 2019. Multi-parameter imaging in the 2016 Mw 7.0 Kumamoto earthquake, Kyushu, Japan and its implications for fluids in seismogenesis. Tectonophysics, v. 767.

Yuan, D., Li, A., 2016. Determination of microseismic event azimuth from S-wave splitting analysis. Journal of Applied Geophysics, v. 137, p. 145-153.

Yuan, D., Li, A., 2017. Determination of microseismic event azimuth from S-wave splitting analysis. Journal of Applied Geophysics, vol. 137, p. 145-153.

Wakita, K., 2013. Geology and tectonics of Japanese islands: A review – The key to understanding the geology of Asia. Journal of Asian Earth Sciences, v. 72, p. 75-87.

Zhang, Z., Schwartz, S. Y., 1994. Seismic anisotropy in the shallow crust of the Loma Prieta segment of the San Andreas Fault System. Journal of Geophysical Research: Solid Earth, vol. 99, p. 9651-9661.

Zhao, D., Tamashita, K., Toyokuni, G., 2018. Tomography of the 2016 Kumamoto earthquake area and the Beppu-Shimabara graben. Scientific Reports, vol. 8, p. 15488.